NmerA, the Metal Binding Domain of Mercuric Ion Reductase, Removes Hg^{2+} from Proteins, Delivers It to the Catalytic Core, and Protects Cells under Glutathione-Depleted Conditions[†,‡]

Richard Ledwidge,[§] Bijal Patel,[∥] Aiping Dong,[⊥] David Fiedler,[∥] Mat Falkowski,[§] Jane Zelikova,[∥] Anne O. Summers,[∥] Emil F. Pai,[⊥,#] and Susan M. Miller*[,§]

Department of Pharmaceutical Chemistry, University of California—San Francisco, 600 16th Street, San Francisco, California 94143-2280, Department of Microbiology, University of Georgia, Athens, Georgia 30602, Departments of Biochemistry, Molecular and Medical Genetics, and Medical Biophysics, University of Toronto, Toronto, Ontario M5S 1A8, Canada, and Division of Cancer Genomics and Proteomics, Ontario Cancer Institute/Princess Margaret Hospital, Toronto, Ontario M5G 2M9, Canada

Received March 22, 2005; Revised Manuscript Received June 28, 2005

ABSTRACT: The ligand binding and catalytic properties of heavy metal ions have led to the evolution of metal ion-specific pathways for control of their intracellular trafficking and/or elimination. Small MW proteins/domains containing a GMTCXXC metal binding motif in a $\beta\alpha\beta\beta\alpha\beta$ fold are common among proteins controlling the mobility of soft metal ions such as Cu^{1+}, Zn^{2+}, and Hg^{2+}, and the functions of several have been established. In bacterial mercuric ion reductases (MerA), which catalyze reduction of Hg^{2+} to Hg^0 as a means of detoxification, one or two repeats of sequences with this fold are highly conserved as N-terminal domains (NmerA) of uncertain function. To simplify functional analysis of NmerA, we cloned and expressed the domain and catalytic core of Tn*501* MerA as separate proteins. In this paper, we show Tn*501* NmerA to be a stable, soluble protein that binds 1 Hg^{2+}/domain and delivers it to the catalytic core at kinetically competent rates. Comparison of steady-state data for full-length versus catalytic core MerA using Hg(glutathione)$_2$ or Hg(thioredoxin) as substrate demonstrates that the NmerA domain does participate in acquisition and delivery of Hg^{2+} to the catalytic core during the reduction catalyzed by full-length MerA, particularly when Hg^{2+} is bound to a protein. Finally, comparison of growth curves for glutathione-depleted *Escherichia coli* expressing either catalytic core, full-length, or a combination of core plus NmerA shows an increased protection of cells against Hg^{2+} in the media when NmerA is present, providing the first evidence of a functional role for this highly conserved domain.

Transition and other heavy metal ions pose an acute toxic challenge to cells because of their propensity for coordination and catalytic reactivity with the functional groups of cellular components (*5*, *6*). To avoid the undesirable consequences of random metal−ligand interactions, living organisms have evolved elaborate mechanisms to control the intracellular trafficking and/or elimination of both essential (e.g., Fe, Cu, and Zn) and nonessential [e.g., Cd^{2+}, Pb^{2+}, Hg^{2+}, and As-(V)] metal ions. Common proteins involved in metal ion trafficking include transmembrane transporters, sequestration/storage proteins, metallochaperones that transport specific metal ions through the cellular milieu and assist in their incorporation into specific metalloproteins, and, occasionally, reductases that catalyze reduction of the metal ions to redox states that are easier to transport or eliminate (*7*−*12*). In contrast to classic metalloproteins where stably bound metal ions provide structure or function to the protein, trafficking proteins have relatively transient interactions with their cognate metal ions. By necessity, interactions in transmembrane transporters and reductase enzymes are completely transient. For storage proteins and metallochaperones, the interactions are state-dependent, i.e., stable until the complex interacts with a specific protein partner to which the metal ion is transferred. Elucidation of the structural and chemical properties of proteins that lead to stable versus transient or state-dependent interactions is of significant interest for understanding the mobility and potential pathways for toxicity of metal ions in biological systems.

Our studies are focused on elucidation of the features of the enzyme mercuric ion reductase (MerA)[1] that facilitate the rapid acquisition and reduction of Hg^{2+} in the cytoplasm of bacterial cells. With its high affinity for thiols as ligands [K_{form} for Hg(thiol)$_2$ reported to be as high as 10^{40} M^{-2} (*3*)] and lability toward rapid exchange of one thiol ligand for

[†] This work was supported by grants from the National Science Foundation (MCB-9982576 to S.M.M.) and the Department of Energy, Office of Science (DE-FG03-01ER63087 to S.M.M., A.O.S., and E.F.P.). This work was also supported by the Canada Research Chairs Program (to E.F.P.).

[‡] The atomic coordinates for the salt form (PDB ID 1ZK7) and for the PEG form (PDB ID 1ZX9) of the Tn*501* MerA catalytic core have been deposited with the Protein Data Bank.

* To whom correspondence should be addressed: phone, 415-476-7155; fax, 415-514-3221; e-mail, smiller@cgl.ucsf.edu.

[§] University of California—San Francisco.

[∥] University of Georgia.

[⊥] Department of Biochemistry, University of Toronto, and Ontario Cancer Institute/Princess Margaret Hospital.

[#] Departments of Molecular and Medical Genetics and Medical Biophysics, University of Toronto.

10.1021/bi050519d CCC: $30.25
Published on Web 08/04/2005

another (*6*, *13*), Hg^{2+} can readily disperse to random protein thiols throughout a cell, causing a general toxicity due to loss of protein function. In the common bacterial resistance pathway involving MerA, this general toxicity is avoided by enzymatic reduction of Hg^{2+} to Hg^0, which having essentially no affinity for ligands simply diffuses from the cell (*8*, *14*−*17*). Since MerA accomplishes this reaction in the thiol-rich environment of the cytoplasm, the protein structure must be designed to effectively compete with the cellular thiols to acquire its Hg^{2+} substrate.

Structurally, MerA proteins are typically composed of two main components: a multidomain catalytic core that is structurally homologous with members of the pyridine nucleotide disulfide oxidoreductase family [e.g., glutathione reductase, trypanothione reductase, and certain thioredoxin reductases (*18*−*21*)] as seen in the crystal structure of the *Bacillus* sp. RC607 enzyme (*22*) and an N-terminal appendage of one or two repeats of a sequence homologous with other "soft" metal ion trafficking proteins/domains (*17*, *23*). Extensive studies of the mercuric ion reductase (MerA) encoded by the transposon *501* (Tn*501*) *mer* operon have shown that the homodimeric catalytic core has two interfacial active sites (*18*, *19*, *24*). In each site, FAD mediates electron transfer between pyridine nucleotide and Hg^{2+} bound to an inner pair of cysteine thiols[2] from one subunit (*25*, *26*). A second pair of cysteine thiols from the C-terminal region of the other subunit serves as a ligand exchange conduit for transfer of Hg^{2+} from thiols in solution to the inner thiols at the site of reduction (*27*−*30*).

The N-terminal domain of the protein (NmerA) also contains a pair of cysteine thiols in a GMTCXXC sequence motif that is conserved in the soft metal ion trafficking proteins that share a common $\beta\alpha\beta\beta\alpha\beta$ structural fold. While several of the related proteins have been shown to bind their cognate metal ion via the cysteine thiols and transfer it to a specific partner, the role of NmerA has remained elusive. Under typical in vitro assay conditions, the N-terminal domain appears to be dispensable (*31*). Furthermore, in vivo analyses showed no effect of mutation of both N-terminal cysteines in MerA to alanines in the context of the full *mer* operon on mercury resistance using either high- or low-copy number plasmids (*29*, *31*, *32*), indicating that NmerA provides no essential role under normal cellular conditions. Despite this, the high degree of conservation of the domain (*17*) and its obvious homology to metallochaperones and other metal binding proteins (*23*) strongly suggest an important function for the domain in metal ion binding and transfer. To simplify investigation of the role of NmerA in the reduction of Hg^{2+} to Hg^0, we have created constructs to express the NmerA domain and the catalytic core[1] of Tn*501* MerA as separate proteins for both in vitro and in vivo studies. While the NMR analysis of NmerA will be described elsewhere (Ledwidge, Dötsch, and Miller, unpublished data), the crystal structure of the Tn*501* core is presented here. Results of in vitro studies described below demonstrate that Tn*501* NmerA is expressed as a stable, soluble, monomeric protein that binds Hg^{2+} in a 1:1 stoichiometric complex[3] and delivers it to the catalytic core of Tn*501* MerA in an efficient manner. In addition, we provide the first evidence that the NmerA domain in the full-length protein does indeed participate in acquisition and delivery of Hg^{2+} to the catalytic core, particularly with bulky $Hg(SR)_2$ complexes when extraneous thiols are depleted. Consistent with the in vitro results, in vivo studies are presented demonstrating the importance of the NmerA domain for increased protection against Hg^{2+} under thiol-depleted conditions in the cell.

EXPERIMENTAL PROCEDURES

Materials. Reagents were from Sigma or Aldrich. BL21-(DE3) pLysS cells and pET vectors were from Stratagene. Top 10 competent cells were from Invitrogen. Restriction enzymes and T4 DNA ligase were from New England BioLabs. Chromatographic supports were from Sigma, Bio-Rad, or Pharmacia. Mimetic Orange 3 from Prometic Biosciences was found as a suitable replacement for the discontinued Orange A resin (Amicon) used in the core and full-length MerA protein preparations. Thioredoxin was from Promega. Protease inhibitor cocktail tablets were from Roche, Inc. The pUB3466bs2 and pJOE114 vectors containing the Tn*501 mer* operon were a kind gift of Prof. Nigel Brown at the University of Birmingham, U.K.

Subcloning and Expression of Catalytic Core and Full-Length MerA. Sequence homology and structures of *Bacillus* MerA (*22*) and human glutathione reductase (*33*) suggest that the fold of the catalytic core of Tn*501* MerA encompasses residues E96 through G561. The corresponding ~1400 bp fragment was amplified by PCR from the full-length *merA* gene in the pJOE114 plasmid using forward primer 5′-CGATTT**CCATGG**AGCCCCCGGTGCAGG-TAGC-3′ (Gibco) to append an initiating ATG Met codon prior to the E96 codon and introduce an *Nco*I site (in bold) and reverse primer 5′-CGC**GGATCC**GTAGGCGTTCAT-TGAACACCTCC-3′ to introduce a *Bam*HI site (in bold) downstream of the stop codon. After digestion of the PCR product and pET-3d vector with *Nco*I and *Bam*HI, the fragments were ligated to generate pET3d:cmerA (Table 1). Transformants of competent BL21(DE3) pLysS *Escherichia coli* with pET3d:cmerA were selected on LB plates containing ampicillin (Amp, 50 μg/mL) and chloramphenicol (Cm, 34 μg/mL) and verified by sequencing. Full-length Tn*501*

[1] Abbreviations: catalytic core, amino acids 1 + 96−561 of Tn*501* MerA; DTNB, dithiobis(2-nitrobenzoic acid); DTT, dithiothreitol; FAD, flavin adenine dinucleotide; GSH, glutathione; GS^-, glutathione thiolate anion; $Hg(SG)_2$, mercuric bis(glutathione anion); $Hg(TNB)_2$, mercuric bis(thionitrobenzoate); K_{form}, formation constant; KP_i, inorganic potassium phosphate; 2-ME, 2-mercaptoethanol; MerA, mercuric ion reductase; MW, molecular weight; NmerA, N-terminal amino acids 1−69 of Tn*501* MerA; RSH, an organic thiol compound; Tn*501*, transposon 501; TNB, thionitrobenzoate; TRX, thioredoxin.

[2] In most pyridine nucleotide disulfide oxidoreductases, FAD mediates electron transfer between pyridine nucleotide and a redox-active disulfide. As isolated, MerA also has a redox-active disulfide that can undergo reduction by this process. However, during catalysis these cysteines remain reduced and are the inner thiols that bind Hg^{2+} during its reduction.

[3] During the course of our work Rossy et al. (*1*) reported the cloning and expression of a stably folded 68 amino acid N-terminal domain from the mercuric ion reductase from *R. metallidurans* and also provided evidence for formation of a 1:1 Hg^{2+} complex of the protein. Their construct was based on both the alignment with MerP sequences and a site for proteolysis between residues 68 and 69 in their protein. In cloning the Tn*501* domain, we made two constructs initially, one for direct expression of the domain and one for expression of the domain fused to an intein (*2*). Since residue 68 is an Asp and the latter would not cleave correctly with Asp immediately before the intein, Ala69 was included in both constructs for consistency.

Table 1: Strains and Plasmids

strain or plasmid	relevant genotype or description	source
AB1157	*E. coli* K12 *ara gal lac mtl xyl arg his leu pro thr rpsL tsx*	*58*
WB821	AB1157 *gshA*	*58*
pDU202	CmlR SulR StrR HgR− Tn*21 mer* operon	*59*
pDG106	KanR HgR− Tn*21 mer* operon	*60*
pET-3, pET-11	AmpR, T7 promoter	commercial (Stratagene)
pET3a:flmerA	pET3a with full-length MerA under T7 promoter	this study
pET3d:cmerA	pET3d with catalytic core MerA under T7 promoter	this study
pET11a:NmerA	pET11a with NmerA under T7 promoter	this study
pASK-IBA3	AmpR, Tet promoter	commercial (IBA)
pFull	pASK with full-length MerA under Tet promoter	this study
pCore	pASK with catalytic core MerA under Tet promoter	this study
pCN	pASK with catalytic core MerA and NmerA under Tet promoter	this study

merA was amplified from pMD01 (*34*) by PCR using the forward primer 5′-GGGAATTC**CATATG**ACCCATCTAA-AAATCACCGGC-3′ to introduce an *Nde*I restriction site (in bold) encompassing the ATG start codon and the same reverse primer used for the catalytic core gene. After digestion of the PCR product and pET-3a vector with *Nde*I and *Bam*HI, the fragments were ligated to generate pET3a:flmerA. Competent BL21(DE3) pLysS cells were transformed with pET3a:flmerA, and colonies were selected and verified as above.

For protein expression of catalytic core and full-length proteins, single colonies from freshly transformed cells were streaked onto LB/Amp/Cm plates, and from these, a single colony was used to inoculate 100 mL of LB/Amp/Cm for overnight growth at 37 °C. One liter cultures of LB/Amp/Cm were inoculated with 20 mL of overnight culture and grown to OD_{600} ~0.7. Protein expression was induced with 400 μM IPTG, and cells were grown for an additional 4 h before being pelleted and stored at −80 °C.

Purification of MerA Catalytic Core. All procedures were performed at 4 °C unless noted. Frozen cultures from 4 L of cells containing pET3d:cmerA were defrosted and resuspended in core Prep buffer (CPB) (20 mM KP_i, pH 7.3, 30 mM cysteine, 1 mM EDTA; 100 mL for sonication or a volume equal to the mass of cells for French press disruption) containing protease inhibitor cocktail (1 tablet/20 mL), 100 μM FAD, and 0.2 mg/mL DNase. Cells were ruptured by sonication (3−5 × 30 s) or by French press, and debris was removed by centrifugation at 40000*g* for 30 min. The supernatant was diluted to 350−400 mL with CPB and loaded over 1−1.5 h onto a CPB-equilibrated Orange 3 (5.5 × 4 cm) column. The column was washed with 1.0 L of CPB and core protein eluted with ca. 200 mL of CPB containing 1 mM $NADP^+$. Yellow fractions were pooled and concentrated to ~5 mL, and the concentrated enzyme was passed through a Sephacryl 200 column (2.5 × 38 cm) equilibrated in CPB to remove high MW protein contaminants and the bulk of the $NADP^+$. At this point or prior to the last step, glycerol may be added to 15% (w/v), and aliquots stored at −80 °C.

Before use, the remainder of the $NADP^+$ was removed by passing concentrated enzyme rapidly (<5 min) through a Sephadex G-50 column (2.5 × 43 cm) equilibrated in CPB + 2 M high purity urea at room temperature. To remove urea, the protein was concentrated to 1−2 mL, FAD (50 μM) added to ensure full reconstitution, and enzyme passed through a Sephadex G-50 column (1.5 × 25 cm) equilibrated in 50 mM KP_i, pH 7.3 at 4 °C. The active site concentration was calculated using a previously determined ϵ_{456} of 11.3 mM^{-1} cm^{-1} (*18*).

Purification of Full-Length MerA. The following procedure was developed to shorten the preparation time so as to minimize the naturally occurring proteolytic cleavage of the NmerA domain from the catalytic core (*18*). Frozen cultures from 4 L of cells containing pET3a:flmerA were defrosted and resuspended in 100 mL of Prep buffer (PB) (50 mM KP_i, 30 mM cysteine, 1 mM EDTA, pH 7.3) containing protease inhibitor cocktail (1 tablet/25 mL) and 0.2 mg/mL DNase. Cells were stirred for 30 min at 4 °C and sonicated 5× for 30 s durations. Cell debris was removed by centrifugation at 40000*g* for 30 min. Supernatant was diluted to 500 mL with PB containing 2 μM FAD and loaded onto an Orange 3 column (6 × 9 cm) equilibrated in PB. The column was washed with 1 L of PB followed by 0.5 L of PB + 0.2 M NaCl. Full-length protein was eluted with 1 L of PB + 1 M NaCl. Yellow protein fractions were pooled and concentrated.

To prepare full-length MerA for kinetic assays, 1 mL of ~10−30 μM freshly prepared enzyme was treated with 5 mM DTT for 30 min on ice. Solid $(NH_4)_2SO_4$ was added to 75% saturation, and the sample was centrifuged at 12000*g* for 10 min at 4 °C. The pellet was dissolved in 1 mL of 50 mM KP_i, pH 7.3, containing 100 μM FAD, and the enzyme was purified by gel filtration on Sephadex G-50 equilibrated in 50 mM KP_i, pH 7.3. The active site concentration was calculated using a previously determined ϵ_{456} of 11.3 mM^{-1} cm^{-1} (*18*).

Properties of Full Length and Core. Both core and full-length proteins were judged to be ~95% pure on SDS−PAGE. The purification protocol for full-length protein yields ~30 mg of protein/L of culture. Because proteolytic cleavage of NmerA from catalytic core is less extensive in fresh preparations, full-length MerA was used immediately for experiments. The purification protocol for core protein yields ~9 mg of protein/L of culture. The activity and UV−vis absorption spectra for oxidized and reduced forms of the full-length protein obtained from this overexpression system are identical to those of protein obtained using the previous overexpression system (*34*) or the *mer* operon (*18*). Likewise, the UV−vis properties of catalytic core are identical to those for the full-length protein.

Crystallization, Data Collection, and Structure Determination of Catalytic Core MerA. Crystals of the Tn*501* MerA catalytic core were grown under two quite different sets of conditions, using the hanging drop vapor diffusion technique. The first crystals were obtained by mixing 2 μL of protein

solution with 2 μL of reservoir solution consisting of 0.1 M sodium acetate, pH 4.4, 6% (w/v) glycerol, and 16% (w/v) PEG 400 as precipitant and equilibrating the drop against 0.5 mL of the reservoir solution at room temperature. Alternatively, glycerol was removed from protein samples by repeated washing in Centricon-30 concentrators with 50 mM KP_i, pH 7.3, after which 2 μL of 25 mg/mL protein solution was mixed with 2 μL of 0.05 M CAPS, pH 9.4, and 1.6 M $(NH_4)_2SO_4$ and the drop then equilibrated against 0.5 mL of this solution at room temperature. Crystals were harvested and transferred to their corresponding reservoir solutions with the concentration of PEG 400 increased to 25% (w/v) for crystals grown in the presence of this precipitant or with 16% (w/v) glycerol added to crystals grown in the presence of $(NH_4)_2SO_4$ for cryoprotection.

Diffraction data sets for both crystal forms were collected at APS, BIOCARS beamline 14BM-C at a wavelength of 0.90 Å equipped with an ADSC Q4 CCD detector. All data sets were processed with the help of the program packages DENZO and SCALEPACK (*35*). The CNS version 1.0 program suite (*36*) was used to solve the structure by molecular replacement and to refine it. The atomic models were generated in the graphics program O (*37*). Parameters for data collection and refinement are summarized in Table S1.

Subcloning and Expression of NmerA. The 207 bp 5′ end of the Tn*501 merA* gene corresponding to the 69 amino-terminal residues was amplified by PCR from the pUB3466bs2 vector using the same forward primer described above for the full-length *merA* gene and the reverse primer 5′-CGC**GGATCC**TCA**T**GCATCGGCTAGC-3′ (Gibco) with introduction of a stop codon, a *Bam*HI site (**GGATCC**), and a silent mutation (C to T) to generate an *Nsi*I site (A**T**GCAT**)** for restriction analysis of the construct. Digestion of the purified PCR product and pET-11a vector with *Bam*HI and *Nde*I, followed by ligation of the fragments, yielded pET11a:NmerA. Transformants of competent *E. coli* BL21(DE3) pLysS cells were selected for growth on LB/Amp/Cm plates at 37 °C and verified by sequencing. Single colonies from freshly transformed cells were used to inoculate 50 mL cultures of LB/Amp/Cm for overnight growth at 37 °C. One liter cultures of LB/Amp/Cm were inoculated with 20 mL of the overnight culture, grown at 37 °C to OD_{600} ~1, and induced by addition of 250 μM IPTG. After 1 h of induction, rifampicin was added to 50 μM to inhibit the *E. coli* RNA polymerase while having no inhibitory effect on the T7 RNA polymerase. Cultures were grown for an additional 4 h before pelleting and storage at −80 °C.

NmerA Purification. Frozen cultures containing pET11a:NmerA were defrosted and suspended (3:1 vol:wet weight) in 50 mM Tris-HCl, pH 8.0, containing 20 mM 2-ME, 1 mM EDTA, protease inhibitor cocktail (1 tablet/50 mL) and lysozyme (0.1 mg/mL). Cells were stirred at 4 °C for 40 min and sonicated on ice 6× for 1 min durations. Cell debris was removed by centrifugation at 40000*g* for 35 min. Streptomycin sulfate (20%) was added slowly to the supernatant (1% w/v, final) and stirred for 30 min at 4 °C. Precipitated nucleic acids were removed by centrifugation at 18000*g* for 35 min. The supernatant was dialyzed 2× for 2 h against 4 L of 25 mM Tris-HCl, pH 8.0, containing 20 mM 2-ME and 1 mM EDTA (TME) at 4 °C, and protein precipitate was removed by centrifugation at 40000*g* for 40 min. Supernatant was loaded onto tandem DEAE (3 × 23 cm) and Fast-Q Sepharose anion-exchange columns (3 × 18 cm) to purify NmerA in the negative binding mode using isocratic elution with TME. Fractions just after the void volume containing NmerA (determined by electrophoresis) were pooled, concentrated to ~5 mL, and loaded onto a P-20 (Bio-Rad) gel filtration column (3 × 110 cm) equilibrated in 25 mM MES, pH 6.0, containing 20 mM 2-ME and 1 mM EDTA (MME) plus 250 mM NaCl. Fractions containing NmerA were pooled, concentrated to ~10 mL, and dialyzed against 4 L of MME for 3 h at 4 °C. Dialyzed protein was loaded onto a Mono-S cation-exchange column (1.8 × 18 cm) equilibrated in MME and eluted using a linear gradient of 0−0.3 M NaCl in MME. Glycerol (10−15%) was added to the protein, which eluted at ca. 75−100 mM NaCl, and samples were stored at −80 °C. Before use, protein was concentrated and transferred into buffer appropriate for the experiment by gel filtration using a P-2 column.

After the three-step purification, NmerA was >95% pure on the basis of electrophoresis using 16.5% Tris−Tricine gels (Bio-Rad). Electrospray mass spectrometry (UCSF) and amino acid analysis (UC Davis) confirmed the identity of NmerA. Elution behavior on the gel filtration column and passage of NmerA through 8 kDa cutoff concentrator membranes were consistent with a monomeric protein. Although a one-column purification has been reported for the domain from *Ralstonia metallidurans* CH34 (*1*), our preparations required the cation-exchange column to remove a higher MW contaminant remaining after gel filtration using the P-20 resin.

$Hg(TNB)_2$ Synthesis. A solution of Na_2HPO_4 (0.6 mmol in 2.9 mL of H_2O) was titrated to pH 12.4 with NaOH and used to solubilize DTNB (0.119 g, 0.3 mmol, 2 equiv of carboxylic acid), giving a solution of Na_2DTNB in >95% yield with a final pH of 7.5. A solution of DTT (0.05 g, 0.3 mmol, 1 equiv of dithiol in 95 μL of H_2O) was added to the solution of Na_2DTNB (0.3 mmol, 1 equiv of disulfide) to generate 2 equiv (0.6 mmol) of TNB dianion ($RCOO^-$ and RS^-) in >90% yield. A solution of $Hg(OAc)_2$ (0.098 g, 0.3 mmol, 1 equiv of Hg^{2+} in 325 μL of H_2O) was added to the solution of TNB dianion (0.6 mmol, 2 equiv of thiol) to generate $Hg(TNB)_2$ in >85% yield. $Hg(TNB)_2$ was purified by size exclusion chromatography using a P-2 resin (Bio-Rad, 0.7 × 25 cm) equilibrated in 10 mM ammonium formate. Fractions containing $Hg(TNB)_2$, identified by their UV−vis absorption spectrum (see Results), were pooled and evaporated to dryness using a rotory evaporator.

Titration of NmerA or TRX with $Hg(TNB)_2$. The protein cysteines of NmerA or TRX were fully reduced by incubation with 5 mM DTT for 1 h at room temperature. Protein was separated from DTT using a P-2 size exclusion column equilibrated with 50 mM KP_i buffer, pH 7.3. Reaction of NmerA or TRX in either 50 mM KP_i buffer, pH 7.3, or 6 M guanidine hydrochloride with DTNB (*38*) confirmed the presence of two thiols per protein monomer. Protein concentrations were determined from the absorbance at 278 or 280 nm using $\epsilon_{278} = 2.55\ mM^{-1}\ cm^{-1}$ for NmerA (see Results) and $\epsilon_{280} = 13.7\ mM^{-1}\ cm^{-1}$ for TRX (*39*). The titration of NmerA or TRX with $Hg(TNB)_2$ was monitored at 412 nm for the release of TNB ligands upon exchange with the protein cysteine thiols.

Table 2: Steady-State Kinetic Constants[a] for the Catalytic Core with Hg−NmerA, Hg−TRX, or $Hg(SG)_2$ and for Full-Length MerA with Hg−TRX and $Hg(SG)_2$

MerA	substrate	GSH (mM)	k_{cat} (s^{-1})	K_{MHg} (μM)	k_{cat}/K_{MHg} (M^{-1} s^{-1} × 10^5)
catalytic core	Hg−NmerA	0.00	12.0 (0.3)	35.1 (3.3)	3.4 (0.3)
catalytic core	Hg−TRX	0.00	7.0 (1.0)	1177 (225)	0.06 (0.01)
full length	Hg−TRX	0.00	9.0 (1.0)	297 (58)	0.3 (0.07)
catalytic core	$Hg(SG)_2$	1.00	8.7 (0.1)	24.0 (1.0)	3.6 (0.2)
		6.25	8.0 (0.1)	27.3 (1.4)	2.9 (0.2)
full length	$Hg(SG)_2$	1.00	9.4 (0.1)	10.7 (0.6)	8.8 (0.5)
		6.25	8.6 (0.3)	21.4 (2.7)	4.0 (0.5)

[a] Steady-state constants were determined from fits of initial velocities to eq 1 using the curve fit routine in Kaleidagraph. Errors (in parentheses) in k_{cat} and K_{MHg} are from the fitting analysis; errors in k_{cat}/K_{MHg} are propagated from those in k_{cat} and K_{MHg} by standard statistical methods.

Steady-State Kinetic Assays. All assays were performed using either a Shimadzu UV-2101PC or a Uvikon XL spectrophotometer furnished with a thermostated cell holder connected to a constant temperature water bath set at 25 °C. Initial rates were monitored by the loss of absorbance at 340 nm due to NADPH oxidation ($\Delta\epsilon_{340} = 6.2$ mM^{-1} cm^{-1}). Reaction conditions held constant for all assays included 50 mM KP_i, pH 7.3, 50 μM NADPH, and 25 nM core or full-length Tn*501* MerA active sites. Assays of core with varied concentrations of Hg−NmerA were run in the absence of other thiols; inhibition of this reaction was examined by analysis in the presence of either 85 or 125 μM reduced NmerA or 100 μM oxidized NmerA. Assays of core and full-length MerA with $Hg(SG)_2$ were examined at varied concentrations of glutathione (see Table 2), and $Hg(SG)_2$ was generated in situ by addition of varied amounts of $HgCl_2$ to the reaction mix containing sufficient GSH to account for that needed to complex the Hg(II) and provide the indicated constant concentration of free GSH. Assays of core and full-length enzymes with varied concentrations of Hg−TRX were run in the absence of other thiols. Assays of core with Hg−TRX in the presence of added NmerA or GSH utilized 60 μM Hg−TRX and varied amounts of NmerA or GSH (see Tables 3 and 4). All reactions were initiated by addition of enzyme to preequilibrated reaction mixtures. Apparent steady-state kinetic constants were determined by fitting the initial rate data to the Michaelis−Menten equation:

$$v = V_{max}S/(K_{MHg} + S) \quad (1)$$

where V_{max} equals the maximal velocity, K_{MHg} is the Michaelis constant for the $Hg(SR)_2$ substrate, and S is the concentration of the $Hg(SR)_2$ substrate. These are apparent constants because NADPH was not varied. However, they are approximately correct since the K_M for NADPH is too low to be measured accurately in our assays but is estimated to be ≤ 5 μM (data not shown).

Construction of Protein Expression Vectors for in Vivo Analysis. Vectors for expression of full-length MerA (pFull) and core MerA (pCore) under control of the Tet promoter (Table 1) were constructed by ligation of the *Bam*HI and *Xba*I restriction fragments of pET3a:flmerA and pET3d:cmerA into the *Bam*HI and *Xba*I cloning site of pASK-IBA3 with T4 DNA ligase (New England BioLabs). Before electroporation into Top 10 competent cells (Invitrogen), the ligated product was digested with *Pvu*II and *Cla*I restriction enzymes to destroy pET3a:flmerA and pET3d:cmerA and with *Sac*II and *Kpn*I to destroy pASK-IBA3 lacking an insert. Transformants were selected for ampicillin resistance and verified by sequencing of both strands.

NmerA was inserted into pCore just 50 nucleotides downstream of the core MerA translational terminator to construct pCN (Table 1) by PCR amplification of the NmerA gene from pET11a:NmerA using 5′-GTCTGCAGCCA-GATCCTCATGCATC-3′ and 5′-GCAGGATCCGAAG-GAGATATACATA-3′ primers (Genosys) with a KOD hot start polymerase (Novagen). The PCR product and pCore were digested with *Bam*HI and *Pst*I followed by ligation with T4 DNA ligase. Before electroporation into Top 10 competent cells, the ligated product was digested with *Xho*I to destroy pCore lacking the NmerA insert. Transformants were selected for ampicillin resistance and verified by sequencing of both strands.

Quantification of Cellular Free Sulfhydryls. A modification of Ellman's method was used to estimate total cellular glutathione (*40*). *E. coli* cultures of 800 mL were grown in A salts minimal media lacking citrate (*41*) and supplemented with 0.2% dextrose, 0.05 μg/mL vitamin B_1, 0.1% casamino acids, 30 μg/mL histidine, and 1 mM $MgSO_4 \cdot 7H_2O$ at 37 °C and 250 rpm. At an OD_{595} of approximately 0.15, cultures were divided, and half were induced for protein expression with 100 μg/L anhydrotetracycline (AHT). Both induced and uninduced cultures were incubated for 1 h as above to an OD_{595} of 0.25−0.35, and cells were harvested by centrifugation at 7000 rpm for 10 min at 25 °C. The cell pellet was suspended in minimal medium at 1% of the original culture volume and divided into four aliquots of 1 mL each. One aliquot was stored at −20 °C for protein determination and immunoassays. Two aliquots received 50 μL of ~10 mM DTNB in 0.1 M phosphate buffer, pH 8.0. The remaining aliquot served as a background control. Cells were lysed by addition of 0.4% chloroform and (4×10^{-3})% SDS with rocking for 10 min at room temperature, and the lysate was cleared of debris by centrifugation at 14000 rpm for 1 min. The supernatant was removed and diluted 11.2-fold in 0.1 M phosphate buffer in duplicates. The A_{412} was read on a Cary 100 Bio UV−vis spectrometer and corrected for the cellular background. Free sulfhydryl content was determined by comparison to glutathione standard curves done at the same time in the same media ($\epsilon_{412} \approx 13000$ M^{-1} cm^{-1}).

Determination of Intracellular Protein Concentrations. Expression of MerA by the constructs, pFull, pCore, and pCN, was determined by quantitative immunoblotting with polyclonal antibody to purified full-length Tn*501* MerA protein. Cultures were grown in Luria−Bertani (LB) broth with 50 μg/mL Amp at 37 °C, 250 rpm, until an OD_{595} of 0.4, at which point a subset of culture was induced with 100 μg/L AHT. After 1 h, cells were centrifuged at 4 °C, 5000 rpm, for 5 min. The cell pellet was suspended in Tris-buffered saline (20 mM Tris·HCl, pH 7.6, containing 136.9 mM NaCl) to its original volume and sonicated on ice for 1 min at half-intensity with pulses of 2−3 s followed by 5 s intervals using a microprobe. After centrifugation at 4 °C, 5000 rpm, for 5 min, the supernatant was mixed with Bio-

Rad Laemmli SDS sample buffer supplemented with 0.2 M DTT. The mixture was heated at 95 °C for 5 min and electrophoresed on Gradipore 12% Tris−glycine I gel at 100 V for ≈1.5 h. The gel was blotted onto Westran S PVDF membrane (Schleicher and Schuell) overnight at 25 V, 4 °C (*41*).

Proteins were detected using a rabbit polyclonal antibody raised against Tn*501* MerA (anti-MerA) and a secondary anti-rabbit antibody from an ECF Western blotting kit according to manufacturer's protocol (Amersham). Proteins were visualized with a Molecular Dynamics, Inc., FluorImager 575 with a 570 nm filter. Densitometry using ImageQuant software was used to determine the amount of protein present in cell lysates compared to a standard curve of pure MerA run on each gel. Cell numbers were determined using the Bradford reagent on cell lysates and values of 156 pg of protein/cell and a 6.7×10^{-13} mL cell volume for *E. coli* (*41*, *42*).

Mercury Resistance Using Efficiency of Plating. Before each experiment, strains were subcultured from −70 °C storage overnight at 37 °C on LB plates. Eight to 10 well-isolated colonies were inoculated into 2 mL of LB broth, 2 mL of LB containing 50 μg/mL Amp, or 2 mL of LB containing 50 μg/mL kanamycin (Kan) as appropriate for each vector, and the cultures were incubated overnight at 37 °C and 250 rpm. Overnight cultures were diluted 1:50 in LB, LB−Amp 50, or LB−Kan 50. The cultures were grown to an OD_{595} of 0.4, at which point 20 mL of each culture was removed and induced. To induce the pFull, pCore, and pCN plasmid strains, anhydrotetracycline (AHT) was added to a final concentration of 100 μg/L and incubation continued for 1 h. To induce pDU202 and pDG106 plasmid strains, $HgCl_2$ was added to a final mercury concentration of 5 μM, and the cells were then incubated for 15 min. A second aliquot of $HgCl_2$ was added to the culture followed by incubation for an additional 5 min. For strains without plasmids and for uninduced plasmids, 20 mL of culture was incubated for either 20 min or 1 h, depending on the time needed for corresponding induced cultures. A final OD_{595} reading for all cultures was taken after the induction period, each culture was diluted to 10^{-2}, 10^{-4}, 10^{-5}, 10^{-6}, and 10^{-7}, and each dilution was spread onto the appropriate plates in duplicate. The plates were incubated overnight at 37 °C. Colonies were counted to determine the efficiency of plating (EOP), i.e., the colonies on the Hg plate divided by those on the LB plate, to determine if any of the strains exhibited mercury resistance. Strains with pDU202 and pDG106 were used as Hg-resistant controls, and the plasmid-less strain was used as an Hg-sensitive control.

Mercury Resistance Phenotype by Growth in Liquid Medium. Before each experiment strains were subcultured from −70 °C storage overnight at 37 °C on LB−agar plates. Eight to 10 well-isolated colonies were inoculated as described above. Overnight cultures were diluted 1:10 in LB. Microtiter plates were prepared with 160 μL per well of the indicated concentrations of $HgCl_2$ in LB and 40 μL of a 1:10 dilution of the appropriate overnight culture. Each strain with each $HgCl_2$ concentration was run in duplicate along with positive and negative controls which behaved as expected. Wells between those containing the cells, were filled with 200 μL of sterile MilliQ water to minimize evaporation from wells during the experiment. An initial OD_{595} reading was taken, and the plate was closed with its lid, placed in a Ziploc bag secured to a shaker platform, and then incubated at 37 °C and 350 rpm. The OD_{595} of each well was read every hour for 8 h. Several lower and higher concentrations of $HgCl_2$ were examined in each experiment, and all experiments were done at least twice. Fifteen micromolar $HgCl_2$ demonstrated the sharpest distinction among all strains.

RESULTS AND DISCUSSION

Overexpression, Purification, and Properties of Catalytic Core MerA. The gene for the 467 amino acid catalytic core region of Tn*501* MerA (initiating M + E96-G561) was cloned by standard PCR techniques and ligated into a pET vector for overexpression under control of the T7 promoter. The protein can be purified in the same manner as full-length protein and exhibits identical spectroscopic and pyridine nucleotide binding properties in its several redox states [data not shown (*18*, *27*)], as well as similar steady-state constants using $Hg(Cys)_2$ as substrate in the presence of 1 mM cysteine [$K_{MHg} = 3-5$ μM and $k_{cat} \sim 12$ s^{-1} (*43*)]. Surprisingly, the yield of the overexpressed catalytic core was significantly lower than yields of full-length protein obtained using vectors with the gene under control of the tac promoter. To test whether the lower expression resulted from differences in the promoter or differences in other properties of the protein constructs, the gene for the full-length protein was also cloned using PCR methods and ligated into a pET vector for overexpression. Yields of purified full-length protein obtained with expression under control of the T7 promoter are similar to those obtained under the tac promoter and are at least 2.5-fold higher than the yield of catalytic core. Further evidence of this disparity is given below using a different expression system.

(A) Crystal Growth. In contrast to the full-length Tn*501* protein, which previously was found to form only low-quality crystals (*22*, *44*), the catalytic core formed diffraction-quality crystals under two quite different conditions. The first one used a reservoir solution of 0.1 M sodium acetate, pH 4.4, 6% (w/v) glycerol, and 16% (w/v) PEG 400 as precipitant whereas the second condition had 0.05 M CAPS, pH 9.4, and 1.6 M $(NH_4)_2SO_4$ in the well solution. For both crystal forms, it took 2−3 days for crystals to reach their final size. The PEG-grown crystals were elongated and about $50 \times 50 \times 500$ μm^3 in size; they belonged to the tetragonal space group $P4_12_12$ and diffracted to about 1.9 Å resolution (see Table S1 for details). The salt-induced crystals grew as diamonds with 200 μm long edges; they adopted space group $P4_32_12$ with a 1.6 Å diffraction limit.

(B) Catalytic Core Structure. Figure 1A shows the 2-fold symmetry of the obligate homodimeric structure from the salt-induced crystal of the Tn*501* MerA catalytic core that is typical of the pyridine nucleotide disulfide reductase family. The overall fold is identical to that observed for the catalytic core of the enzyme isolated from *Bacillus* sp. strain RC607, which was the only part observable in the crystal structure of that enzyme (*22*). The same is true for the PEG crystals. Figure 1B shows a side view of the dimer highlighting the position of the active site FAD and inner cysteine sulfurs deep in the protein and the C-terminal tail folded into a large cleft that opens to the same surface (Figure 1A) as the N-terminus of the protein to which the NmerA domain

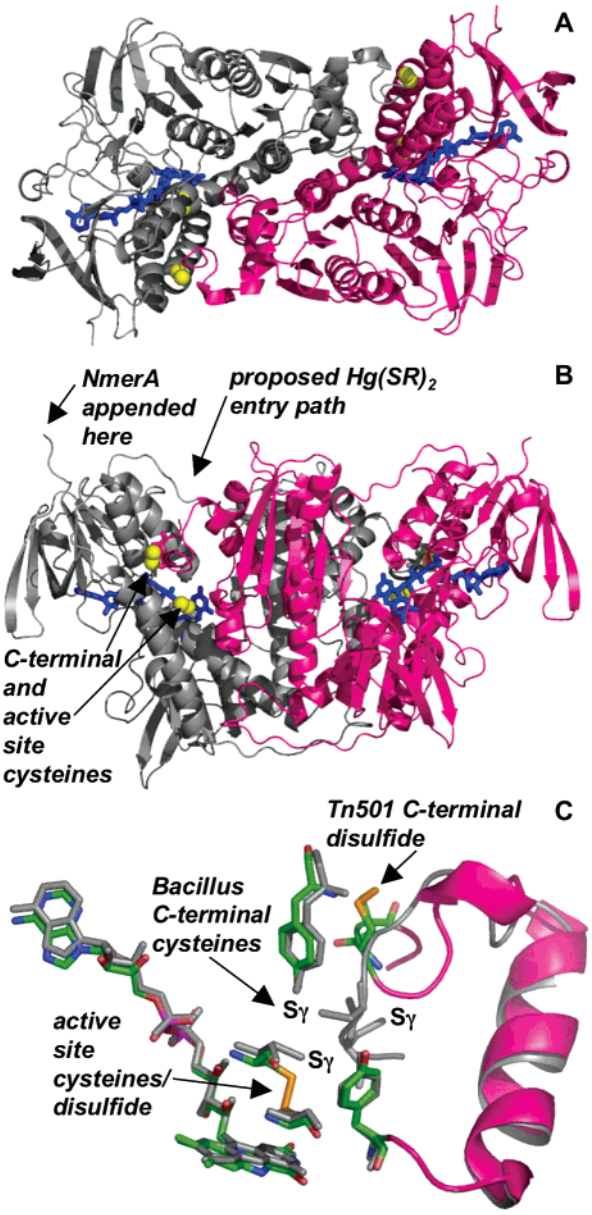

FIGURE 1: Ribbon representation of the dimer of the oxidized Tn*501* MerA catalytic core (salt form, PDB ID code 1ZK7). (A, B) The two subunits are color-coded in gray and pink, FAD molecules are shown as stick models in blue, and the sulfurs of the inner and C-terminal cysteine pairs are shown in space-filling representation in yellow. (C) Overlay of the active sites of the reduced form of MerA from *Bacillus* sp. RC607 with the oxidized form of core MerA from Tn*501*. FAD, inner cysteines, tyrosines, and C-termini of the *Bacillus* MerA are all in gray; the corresponding Tn*501* residues are in pink and standard atom colors. Figures were rendered in Pymol.

is normally appended via a linker (25 amino acids in the Tn*501* protein), suggesting a "swinging arm" mechanism. Although there is a very slight difference in the orientation of the monomers in the Tn*501* and *Bacillus* MerA dimers, the active sites are still well conserved (Figure 1C). The major differences between the three crystal structures were found in the 12 amino acid C-terminal segments which include the pair of cysteines that participates in the initial ligand exchange with the $Hg(SR)_2$ substrate (*30*). In the electron density for the crystal of the reduced *Bacillus* protein, all but the last amino acid could be defined, but the *B*-factors for atoms in this region were overall higher than those for most of the protein, suggesting some flexibility of this region. In the PEG crystals of the Tn*501* protein, the last 11 amino acids were not well ordered and only visible as disconnected patches in the electron density map. In the electron density for the salt-induced crystals of the oxidized Tn*501* protein, the entire 12 amino acid segment assumed a clearly defined structure, but the C-terminal cysteine sulfurs were oxidized to an inactive disulfide, and an ordered sulfate ion and glycerol molecule were also present (see Figure S1). Comparison of the structure shown here with several mutant Tn*501* core structures (Dong, Liu, Miller, and Pai, unpublished results) indicates that the sulfate and glycerol molecules displaced the last 4−6 residues from a position closer to that seen in the *Bacillus* MerA structure (Figures 1C and S1), which together with the inactive state of the C-terminal cysteines raises the uncertainty of the relevance of the exact position observed in this structure. However, the structural flexibility observed in the C-terminus is consistent with the expectation that this region needs to be mobile to allow the C-terminal cysteines to both access the incoming $Hg(SR)_2$ substrate and then deliver it to the buried inner cysteine pair for reduction.

Overexpression, Purification, and Properties of NmerA. The gene for the 69 amino acid N-terminal region[3] (NmerA) of Tn*501* MerA was cloned using standard PCR techniques and ligated into a pET vector for overexpression. A three-step purification procedure yielded ~20 mg of pure protein/L of culture. The mass spectrum of the protein and its amino acid analysis corresponded exactly with the predicted peptide sequence including the N-terminal methionine in at least 50% of the protein (data not shown). Comparison of the amino acid analysis with the UV absorbance of a sample of purified protein gave an extinction coefficient at 278 nm (ϵ_{278}) of 2.55 $mM^{-1}cm^{-1}$, close to the value expected for a polypeptide containing two tyrosines (*45*). The UV−vis absorption spectrum of homogeneous NmerA showed no peaks beyond 278 nm, indicating no chromophores were bound. NMR structural studies conclusively demonstrated the presence of both secondary and tertiary structure (*46*; Ledwidge, Dötsch, and Miller, unpublished results). All of these data indicate that NmerA expressed separately from the catalytic core of Tn*501* MerA is a stable, soluble, folded protein with both secondary and tertiary structure and therefore is suitable for study independent from the catalytic core. This is also consistent with a recent report of the structure of the N-terminal domain of the MerA isolated from *R. metallidurans* CH34 that was determined using residual dipolar coupling NMR methods (*1*).

(A) $Hg(TNB)_2$ Synthesis and Hg−NmerA Complex Formation. In previous efforts to characterize the stoichiometry of Hg^{2+} binding to the conserved GMTCXXC motif in the NmerA homologue MerP (the periplasmic Hg^{2+}-binding protein from the *mer* operon), titration or dialysis of the protein against $HgCl_2$ typically gave Hg^{2+}:MerP stoichiometries in excess of 1:1, indicating adventitious binding of Hg^{2+} to residues other than the two cysteine thiols in the protein (*47*). To avoid this adventitious binding in NmerA, a $Hg(TNB)_2$ complex was used for titration with the expectation that the resonance-stabilized thiolate anion (pK_a ~5.0) of TNB should be a weaker ligand for Hg^{2+} than the chelating Cys_{11}, Cys_{14} dithiol of NmerA[4] (typical Cys pK_a 8−10) but a stronger ligand than amino groups, which have

Scheme 1: Strategy for the Synthesis of $Hg(TNB)_2$

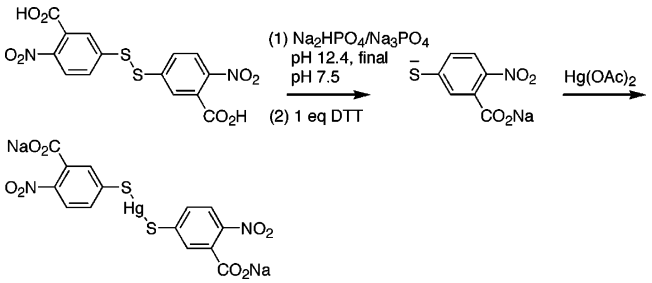

the next highest affinity for Hg^{2+} among available functional groups in proteins [$Hg(NH_3)_2^{2+}$: log K_f = 17.5 (*4*)]. In addition, this complex has previously been generated in situ and found to undergo a spectroscopic change upon metal ion binding/dissociation that can be used to monitor the ligand exchange reaction (*48*). Since the complex had not previously been isolated, we developed the synthesis (Scheme 1) and purification described in Experimental Procedures. As shown in Figure 2A, $Hg(TNB)_2$ exhibits a λ_{max} at 354 nm, intermediate between that of DTNB (324 nm) and TNB (412 nm), suggesting the presence of greater electron density on the S in the Hg−S bond than in the disulfide of DTNB or in the H−S bond of protonated TNB (λ_{max} = 330 nm). The extinction coefficient for $Hg(TNB)_2$ at 354 nm (ϵ_{354}) was determined to be 20.8 $mM^{-1}cm^{-1}$. Addition of 2 equiv of a thiol with a higher pK_a, such as cysteine or glutathione, rapidly and quantitatively released both TNB ligands from 1 equiv of $Hg(TNB)_2$, indicating a substantially weaker affinity of the lower pK_a thiol for Hg^{2+} as predicted (data not shown).

Fully reduced NmerA was titrated with $Hg(TNB)_2$ as shown in Figure 2B. Addition of 1 equiv of $Hg(TNB)_2$ to 1 equiv of NmerA released 2 equiv of TNB. Further addition of $Hg(TNB)_2$ gave no further release of TNB, the difference spectrum (inset, Figure 2B) showing only the presence of the added $Hg(TNB)_2$ (peak at 354 nm). This clearly demonstrates that the TNB ligands bound to Hg^{2+} were exchanged for the higher affinity cysteine thiols of NmerA with formation of a 1:1 Hg−NmerA complex. [A 1:1 complex has also been demonstrated for the domain from *R. metallidurans* (*1*).] That the thiols (rather than other potential ligands) were complexed was verified by the observation that the purified Hg−NmerA complex no longer reacted with DTNB. In addition, electrospray mass spectral analysis of the purified complex demonstrated the presence of one bound Hg^{2+} per monomer (data not shown). The release of only 2 equiv of TNB per monomer of NmerA further indicated that no other functional groups in the protein have a high enough affinity to displace the TNB thiolates from Hg^{2+}, making this a highly specific reagent for titrating available protein thiol groups.

(B) Kinetics of Delivery of Hg^{2+} to the Catalytic Core of Tn501 MerA by Hg−NmerA. To determine whether Hg−NmerA can deliver the metal ion to the catalytic core for reduction, the complex was tested as a substrate for the core in steady-state turnover. Typical in vitro steady-state kinetic assays of the enzyme are performed in the presence of an excess of thiol ligands for Hg^{2+} (e.g., glutathione or cysteine), in part to mimic the cellular environment where small molecular weight thiols such as glutathione are present at millimolar levels and in part to avoid formation of a covalent adduct of Hg^{2+} with NADPH (*49*). However, these conditions are not ideal for evaluation of the ability of Hg−NmerA to directly hand Hg^{2+} to the core, since equilibration of the complex with other thiols would obscure the conclusion. Since no formation of the Hg−NADPH adduct (which leads to loss of 340 nm absorbance) was found upon mixing NADPH with Hg−NmerA, analysis of the steady-state reaction of NADPH with Hg−NmerA as the substrate for the core in the absence of excess thiol was pursued. As illustrated in Figure 3, Hg−NmerA behaved like a typical substrate showing classical saturation kinetics with k_{cat} and k_{cat}/K_{MHg} values comparable to those obtained using low MW $Hg(SR)_2$ substrates, an important point discussed further below (Table 2). This is the first demonstration that NmerA can hand off Hg^{2+} directly to the catalytic core of Tn*501* MerA for subsequent two-electron reduction.

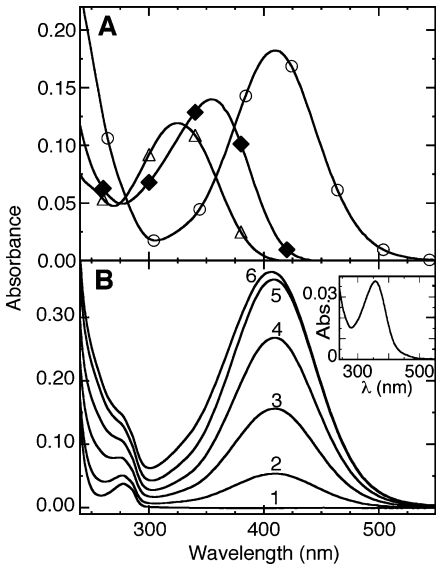

FIGURE 2: (A) UV−vis absorption spectra (1 cm path length) of (△) 6.7 μM DTNB (ϵ_{324} = 17.8 mM^{-1} cm^{-1}), (○) 13.4 μM TNB (ϵ_{412} = 13.6 mM^{-1} cm^{-1}), and (◆) 6.7 μM $Hg(TNB)_2$ (ϵ_{354} = 20.8 mM^{-1} cm^{-1}) in 50 mM KP_i buffer, pH 7.3. (B) Titration of (1) NmerA (15 μM in 50 mM KP_i, pH 7.3; 1 cm path length) with aliquots of (2) 2 μL, (3) 6 μL, (4) 10 μL, (5) 14 μL, and (6) 16 μL of 1 mM $Hg(TNB)_2$ in 50 mM KP_i, pH 7.3, monitored at 412 nm by release of TNB (ϵ_{412} = 13.6 mM^{-1} cm^{-1}). Titration was complete upon addition of 1 equiv of $Hg(TNB)_2$, yielding a 1:1 Hg−NmerA complex. Inset: Difference spectrum (6 − 5) showing the presence of remaining 1 μM $Hg(TNB)_2$ at the end of the titration.

Comparison of the Kinetic Constants for Catalytic Core and Full-Length MerA with Other $Hg(SR)_2$ Substrates. With the observation that NmerA does indeed bind and deliver Hg^{2+} to the catalytic core, we returned to the question of whether full-length enzyme with NmerA appended exhibits any perceptible differences in its kinetic behavior compared with the catalytic core. In earlier studies of the enzyme, comparison of the steady-state kinetic constants for full length versus protein that was proteolytically clipped in the

[4] The numbering of the cysteines in the Tn*501* protein has varied in the literature, with some numbers derived from the sequence including the N-terminal Met and others derived from the sequence lacking it. In this paper we have consistently numbered the residues using the sequence including the N-terminal Met. Hence, N-terminal cysteines in NmerA are 11 and 14, the redox-reactive cysteines, which have been numbered as 135 and 140 in all of the former literature, are here numbered as 136 and 141, and the C-terminal cysteines are 558 and 559.

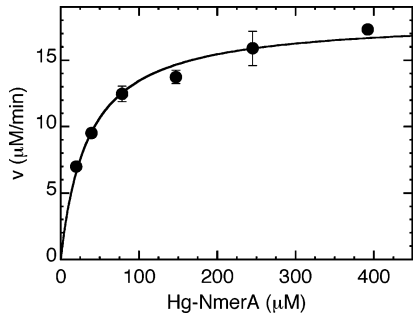

FIGURE 3: Initial velocities of NADPH oxidation by catalytic core MerA using Hg−NmerA as substrate in the absence of small MW thiols. Reactions were performed in triplicate as noted in Experimental Procedures. Some error bars are smaller than the symbols. The solid line shows the fit of the data to eq 1, yielding $V_{max} = 18 \pm 0.45$ μM/min and $K_{MHg} = 35.1 \pm 3.3$ μM.

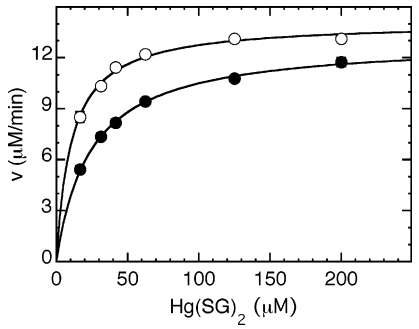

FIGURE 4: Initial velocities of NADPH oxidation catalyzed by catalytic core (●) and full-length MerA (○) using $Hg(SG)_2$ as substrate in the presence of 1 mM GSH. Reactions were performed in duplicate as noted in Experimental Procedures. Most error bars are smaller than the symbols. Curves show fits to eq 1, yielding values for V_{max} and K_{MHg} in Table 2.

linker between NmerA and the catalytic core showed no apparent difference (*31*). However, the importance of the redox state of the several cysteine thiols in the proteins was not well understood at the time and was not carefully controlled in those experiments: only two reduced thiols/subunit were reported rather than the six expected for full length or four for the proteolytically clipped enzyme (*31*). The low thiol titer is indicative of oxidation of the C- and N-terminal dithiol pairs to disulfides or beyond (*27*). Cysteines oxidized beyond the disulfide state cannot be rereduced under the assay conditions and cannot participate in the reaction. The disulfide of the C-terminal pair can be reduced slowly by NADPH via the inner dithiol pair to give partially activated enzyme (*27*), but reduction of a disulfide in the NmerA domain does not occur in the time frame of the assays (*27*). Thus, it is likely that the full-length protein used in the earlier studies lacked the fully reduced NmerA cysteine thiols needed to participate in Hg^{2+} binding, making the results an invalid test of their functionality. For the kinetic studies reported here, the enzymes were freshly prepared, assayed the same day for thiol content, and used immediately only if the thiol titer was ≥3.5 thiols/subunit for catalytic core or ≥5.6 for full length and the latter was ≥80% intact as judged by SDS−PAGE.

(A) Comparison Using $Hg(SG)_2$ as Substrate at Varied Free [GSH]. For comparison of the steady-state kinetics of catalytic core versus full-length MerA, the Hg^{2+} complex with glutathione (GSH) was evaluated since this is expected to be the most prevalent low MW $Hg(SR)_2$ complex that Tn*501* MerA would encounter in the cell. This is also in contrast to various earlier studies where Hg^{2+} was complexed with either 2-mercaptoethanol (*31*) or cysteine (*43*), a point discussed further below. As mentioned above, assays with Hg^{2+} complexes of low MW thiols include an excess of the thiol ligand, in principle to mimic physiological conditions of excess thiol, but typically set at only 1 mM. Since physiological concentrations of GSH in *Pseudomonas aeruginosa* (from which Tn*501* MerA was originally isolated) range closer to 6 mM, the steady-state behavior with $Hg(SG)_2$ as substrate was evaluated both at the lower concentration of 1 mM and at the more physiologically relevant concentration of 6.25 mM excess GSH. As indicated in Table 2, the k_{cat} values for core and full-length proteins are very similar under both conditions. However, the k_{cat}/K_{MHg} values differ for the two enzymes with the difference being substantially greater at the lower thiol concentration as seen in Figure 4. At 6.25 mM GSH, the full-length k_{cat}/K_{MHg} value is only 38% greater than the core value, while at the lower GSH concentration, the full-length value is ca. 144% greater than the core value (Table 2). The observation that the kinetics differ at all provides the first evidence that the appended NmerA domain in the full-length protein can indeed participate in the acquisition and delivery of Hg^{2+} to the catalytic core.

(B) Expected Distribution of Hg^{2+} in Low Thiol Environment. The increased kinetic impact of appended NmerA observed at lower than normal thiol concentrations suggests that participation of NmerA may be important primarily under conditions where the intracellular GSH concentration is diminished. With less GSH to compete, increased binding of Hg^{2+} to other protein thiols would be expected, particularly to proteins with two or more thiols available to chelate the metal ion. An example of such a protein is thioredoxin (TRX), a small, ubiquitous protein with a pair of redox-active cysteine thiols that modulate a variety of cellular processes through control of protein thiol/disulfide oxidation states (*50*). Many proteins whose biological activities are controlled by reduction of a disulfide to a dithiol are highly specific for TRX as the reductant even though GSH at physiological concentrations has a similar reduction potential (*51*). Thus chelation of Hg^{2+} by the dithiol of TRX should be highly detrimental to a number of cellular processes and efficient removal of bound Hg^{2+} critical. The question of interest here is whether the C-terminal thiols on the catalytic core can access Hg^{2+} from a protein such as TRX at all and to what extent NmerA versus GSH can facilitate the process.

(C) Comparison of Full-Length and Catalytic Core Kinetics Using Hg−TRX as Substrate. To address the question, a 1:1 Hg−TRX complex was generated as a test substrate by stoichiometric titration of reduced *E. coli* TRX with $Hg(TNB)_2$ (data not shown) and evaluated as a substrate in two types of experiments. In the first experiment, the Hg−TRX complex was examined as a substrate in steady-state assays with the core and full-length MerA in the absence of GSH. As summarized in Scheme 2, the steady-state k_{cat}/K_{MHg} constants for full length and core both reflect the initial thiol ligand exchanges in the transfer of Hg^{2+} from the donor protein to MerA, but since the paths differ, the magnitudes of the constants in the two proteins should reflect differences in the initial second-order rates of interaction of the NmerA

Scheme 2: Comparison of Hg^{2+}−Ligand Exchange Pathways for Full-Length (Outer Pathway) and Catalytic Core (Lower Pathway) MerA[a]

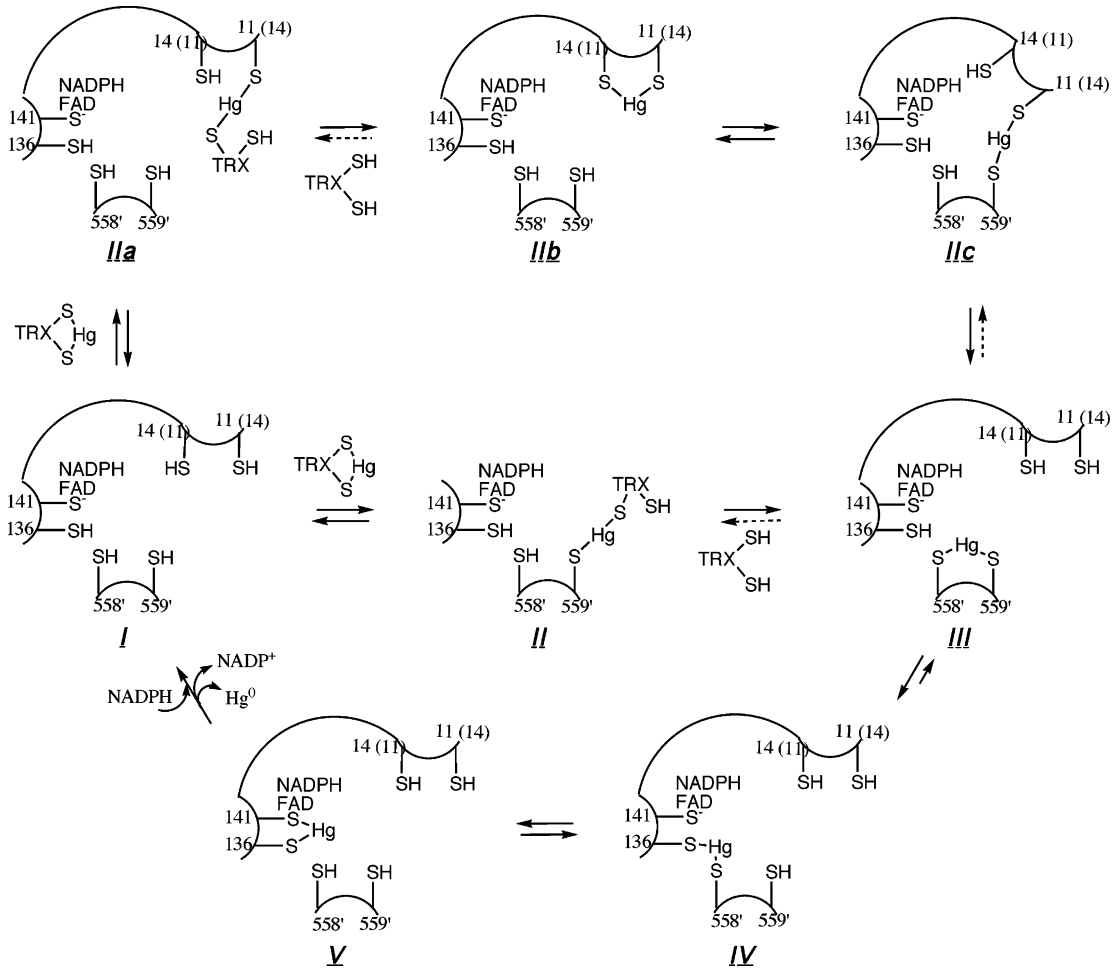

[a] With Hg−protein substrates, the initial exchange occurs with appended NmerA in the full-length protein and is followed by internal transfer to the C-terminal thiols. Since k_{cat}/K_{MHg} only includes steps from the initial encounter through the first irreversible step, it will primarily be limited by the interchanges from species **I** → **IIa** → **IIb** (and possibly **IIc**) for the full-length protein, and k_{cat} may be limited by all forward steps from **IIa** to **I** via the full-length pathway. In the catalytic core, initial exchange occurs directly with the C-terminal thiols, and k_{cat}/K_{MHg} will primarily be limited by the interchanges from species **I** → **II** → **III**, while k_{cat} may be limited by all forward steps from **II** → **I** though the core pathway.

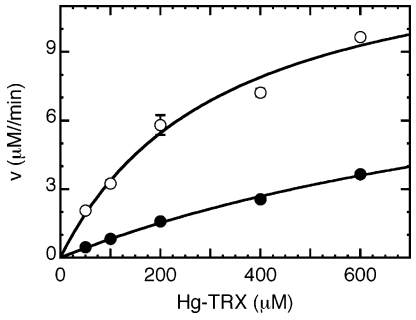

FIGURE 5: Initial velocities of NADPH oxidation catalyzed by catalytic core (●) and full-length MerA (○) using Hg−TRX as substrate in the absence of small MW thiols. Reactions were performed in duplicate (except at 600 μM) as noted in Experimental Procedures. Some error bars are smaller than the symbols. Curves show fits to eq 1, yielding values for V_{max} and K_{MHg} in Table 2.

versus C-terminal thiols with the TRX-bound Hg^{2+} (i.e., kinetic accessibility) as well as differences in the partitioning of the Hg-bound intermediates in each case. Figure 5 shows that although the C-terminal thiols of core can acquire Hg^{2+} directly from TRX at a very low rate, appended NmerA does provide a significant kinetic advantage manifest as a 5-fold greater k_{cat}/K_{MHg} for full-length versus core protein (Table 2), consistent with a greater accessibility of the thiols on the small appended NmerA domain to the TRX-bound Hg^{2+} in solution. The surprisingly modest magnitude of the rate enhancement may be an indication that the increased accessibility of the NmerA-bound Hg^{2+} also leads to a greater back-partitioning of the reaction in full-length protein due to attack by TRX. Regardless, the definitive rate enhancement observed here strongly suggests a role for NmerA in facilitating acquisition of Hg^{2+} from other proteins under low thiol conditions.

In contrast to the above comparison, which measures accessibility of different MerA thiols to the same protein-bound Hg^{2+}, comparison of the k_{cat}/K_{MHg} values for Hg−NmerA versus Hg−TRX as separate substrates for core (Table 2) provides a direct measure of the ability of the core thiols to access Hg^{2+} from two structurally different proteins. The 56-fold higher value for Hg−NmerA suggests that the cognate partners NmerA and core have evolved a specific interaction that facilitates rapid transfer of Hg^{2+}. As shown in Figure 1B, NmerA is appended to the surface of the core near the opening to the trough in which the reduced

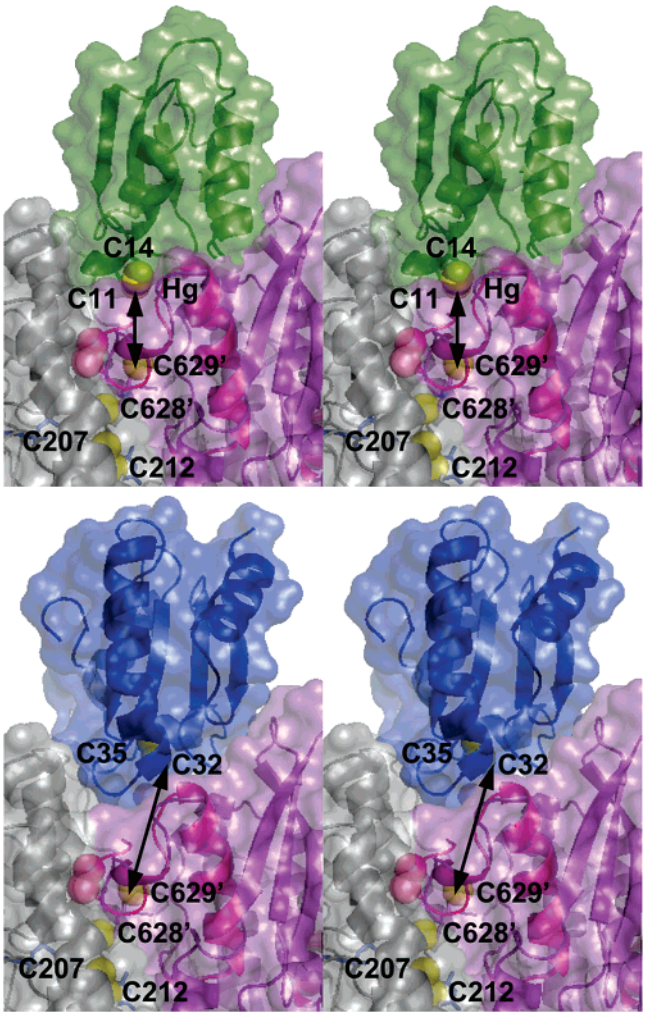

FIGURE 6: Stereoview of the structure of reduced *Bacillus* sp. RC607 MerA (gray, purple) docked with (top) Tn*501* Hg−NmerA (green; Ledwidge, Dötsch, and Miller, unpublished results) or (bottom) *E. coli* TRX (blue; PDB code 2TRX). Using the program Chimera (UCSF), structures were manually docked as rigid bodies to minimize the distance (shown by arrows) between the observed position of the MerA C-terminal cysteine sulfur (C629′) and Hg-(II) in NmerA (∼9.5 Å) or the most accessible cysteine (C32) in TRX (∼15 Å) without infringement of van der Waals surfaces. The *Bacillus* MerA (C207, C212, C628′, C629′), NmerA (C11, C14), and TRX (C32, C35) sulfurs are shown as yellow spheres, and Hg(II) is shown as a black sphere. For comparison, the C-terminus of the Tn*501* catalytic core with the oxidized (disulfide) C464 and C465 sulfurs as spheres is overlaid in pink. Figures were rendered in Pymol.

C-terminal cysteines are observed in both the *Bacillus* MerA structure (*22*) and several mutant Tn*501* core MerA structures (Dong, Pai, and Miller, unpublished results), suggesting the two may interact through that opening. Figure 6 shows hypothetical models of Hg−NmerA (top; Ledwidge, Dötsch, and Miller, unpublished results) and TRX (bottom) docked manually as rigid bodies to the opening to the trough in the core of the *Bacillus* MerA minimizing the distance between the C-terminal cysteine (C629′) and either the Hg in Hg−NmerA or C32 in TRX without violating the van der Waals surfaces. The *Bacillus* MerA was used for the docking as it better illustrates the position of the *reduced* C-terminal cysteines we observe in both proteins, but the position of the oxidized C-terminal cysteines observed in the Tn*501* structure presented here is also shown for comparison.

Table 3: Increase in Initial Rates (v) Observed upon Addition of GSH to Reaction of Core with 60 μM Hg−TRX

GSH (μM)	max $Hg(SG)_2$ (μM)[a]	max expected v (μM/min)[b]	obsd v (μM/min)[c]	calcd $Hg(SG)_2$ (μM)[d]
50.0	25.0	6.1 ± 0.2	1.5	3.4 ± 0.2
100.0	50.0	8.0 ± 0.2	1.8	4.2 ± 0.2
250.0	60.0	8.5 ± 0.2	3.4	9.5 ± 0.5
500.0	60.0	8.5 ± 0.2	4.6	15.0 ± 0.8
1000.0	60.0	8.5 ± 0.2	7.2	36.7 ± 2.1

[a] Concentration of $Hg(SG)_2$ that would result from full transfer of Hg^{2+} from Hg−TRX to the added thiol. [b] Maximal expected values for v were calculated from eq 1 using the steady-state constants from Table 2 and the indicated maximal $Hg(SG)_2$. [c] Observed v is reported as the rate observed after addition of thiol minus the rate with core and Hg−TRX alone, which was 1 μM/min. [d] Concentration of $Hg(SG)_2$ calculated from the observed increases in velocity and the steady-state constants in Table 2.

Although only hypothetical, the models suggest that the smaller size of NmerA allows it to enter the trough to a greater extent than the broader TRX, thereby placing the bound Hg(II) much closer (ca. 9.5 Å in this model) to C629′ than would occur in TRX (ca. 15 Å to the outer C32 in this model) and allowing a more efficient transfer from Hg−NmerA. Specific interactions between residues on core and NmerA are also likely to contribute to a more efficient transfer, and mutagenesis studies are underway to explore this further.

In one final comparison, we note that, in the context of the full-length protein, the transfer of Hg^{2+} from appended NmerA to the core is part of the first-order (k_{cat}) processes rather than part of the second-order (k_{cat}/K_{MHg}) process of acquisition of Hg^{2+} from TRX (Scheme 2). Hence, initiation of Hg^{2+} transfer from Hg−TRX via NmerA contributes the additional steps of transfer between the NmerA and C-terminal thiols to the first-order k_{cat} term. The fact that the apparent k_{cat} (Table 2) for the full-length protein is as fast as or faster than that for the core with Hg−TRX despite the inclusion of the additional steps for transfer of Hg^{2+} between domains provides further evidence for a specific interaction between the two domains that leads to a very efficient transfer of Hg^{2+} between their thiol pairs.

(D) Enhancement of Reaction of Catalytic Core with Hg−TRX by GSH or NmerA. Having shown that appended NmerA provides at least a 5-fold kinetic advantage over core in acquisition of Hg^{2+} from Hg−TRX, the next question of interest is whether GSH can facilitate the reaction of core with Hg−TRX and, if so, how much is required to achieve a similar rate enhancement to that provided by appended NmerA in the absence of GSH. Since the core exhibits a 55-fold higher k_{cat}/K_{MHg} value with $Hg(SG)_2$ versus Hg−TRX (Table 2), enhancement of the initial velocity upon addition of GSH to a reaction of core with Hg−TRX is expected if GSH can rapidly equilibrate with Hg−TRX to yield $Hg(SG)_2$. The magnitude of the resulting velocity then will depend on both the affinity of GSH for Hg^{2+} relative to TRX and the kinetic constants that define the reaction of core with $Hg(SG)_2$ (k_{cat} and K_{MHg} in Table 2). Table 3 summarizes the effect of varied concentrations of GSH on the reaction of 60 μM Hg−TRX and 50 μM NADPH with 25 nM core. The initial rate for the reaction in the absence of GSH was 1 μM/min. Hence, to achieve the same 5-fold

Table 4: Increase in Initial Rates (v) Observed upon Addition of NmerA to Reaction of Core with 60 μM Hg−TRX[a]

NmerA (μM)	max Hg−NmerA (μM)	max expected v (μM/min)	obsd v (μM/min)	calcd Hg−NmerA (μM)
25.0	25.0	7.5 ± 0.5	7.9	27.4 ± 2.8
50.0	50.0	10.6 ± 0.6	10.0	44.0 ± 5.0

[a] All headings as described in Table 3, but with Hg−NmerA in place of $Hg(SG)_2$.

enhancement provided by appended NmerA required a concentration of ≥500 μM GSH. However, as demonstrated above, full-length protein would still be more effective than core at these low [GSH] as it shows a 2.5-fold higher k_{cat}/K_{MHg} with $Hg(SG)_2$ (Table 2). Thus when GSH is depleted, appended NmerA will provide the double advantage of a higher rate of reaction directly with the protein-bound Hg^{2+} complex and a higher rate of reaction with whatever $Hg(SG)_2$ that is formed at equilibrium.

As emphasized above, the increase in velocity upon addition of GSH to the Hg−TRX reaction is expected if $Hg(SG)_2$ is formed in rapid equilibrium with Hg−TRX. Thus, to a first approximation, the measured velocities along with the steady-state constants from Table 2 can be used to estimate the actual concentration of $Hg(SG)_2$ formed at each GSH concentration (Table 3), and these in turn can be used to obtain rough estimates of the relative affinity of the TRX and GSH thiols for Hg^{2+}:

$$Hg(SG)_2 + TRX \overset{K_{eq1}}{\rightleftharpoons} 2GSH + Hg{-}TRX \qquad (2)$$

As shown in Table 3, the observed increases in rate are substantially lower than expected for full transfer of Hg^{2+} to GSH and indicate that the equilibrium clearly favors Hg−TRX, as expected for competition between a monodentate and a bidentate ligand. From the calculated concentration of $Hg(SG)_2$ formed at each [GSH], an average value of 25 ± 12 mM is estimated for K_{eq1} in eq 2.

To obtain a measure of the relative affinity of the NmerA versus TRX thiols, the same experiment was conducted, but with separate reduced NmerA added to enhance the rate of reaction of core with Hg−TRX. As shown in Table 4, the observed increases in rate obtained with reduced NmerA are within experimental error of the expected values at both concentrations examined, indicating a nearly maximal transfer of Hg^{2+} from the TRX dithiol to NmerA upon mixing. The slightly lower than expected velocity at 50 μM NmerA corresponds to a Hg−NmerA concentration of ca. 44 ± 5 μM, still roughly 90% transfer at nearly equimolar NmerA and TRX (50 versus 60 μM total). The results clearly indicate an overall equilibrium that favors Hg−NmerA and give a lower estimate for K_{eq2} in eq 3 of at least 7. Combining eqs

$$Hg{-}TRX + NmerA \overset{K_{eq2}}{\rightleftharpoons} TRX + Hg{-}NmerA \qquad (3)$$

2 and 3 provides a lower estimate for the equilibrium between $Hg(SG)_2$ and Hg−NmerA in eq 4 at ca. 175 mM. Although

$$Hg(SG)_2 + NmerA \overset{K_{eq3}}{\rightleftharpoons} 2GSH + Hg{-}NmerA \qquad (4)$$

the propagated errors in the estimates for the equilibrium constants are substantial, the results clearly demonstrate that the affinity of these thiol compounds for Hg^{2+} follows the order NmerA > TRX > GSH.[5] Thus, the structure of NmerA appears to provide both kinetic accessibility and a thermodynamic sink for accumulation of Hg^{2+} from other thiol-containing species in the cellular milieu. Overall, these results strongly suggest that, in a state of depleted low MW thiol, the presence of appended NmerA should substantially improve the rate of elimination of Hg^{2+} bound to proteins and, hence, increase the chances for cell survival.

(E) Evaluation of the in Vivo Impact of NmerA on Cell Survival. Previous studies had shown that the full *mer* operon expressing full-length MerA confers mercury resistance on *E. coli* depleted in glutathione (*52*). Thus, to explore the proposed role of NmerA in cells, full-length MerA versus catalytic core alone or core coexpressed with NmerA were evaluated for their ability to allow a strain of *E. coli* depleted in glutathione (Table 1) to grow in the presence of $HgCl_2$ in the media. Since the *gshA*$^-$ mutant host (WB821) and its parent AB1157 strain lack the gene for T7 RNA polymerase, the MerA derivatives were first moved from the pET vectors to the pASK vector to allow inducible gene expression under control of the Tet promoter (Table 1). As summarized in Table 5, quantification of protein expression by immunoblotting revealed considerable leaky expression of both core and full-length MerA proteins from these constructs but a further increase in concentration by at least 5-fold upon induction with AHT in both cell lines. More important to the phenotypic analysis, expression of full-length MerA (induced or uninduced) was found to be much greater than that of core MerA, even though all of the vectors have the same promoter and ribosome binding site. This is consistent with the differential yields of purified full-length and core proteins obtained with the pET expression system noted above and suggests that appended NmerA confers some stability on the folded protein. However, coexpression of NmerA (although not verifiable by immunoblotting but implicated by the phenotypic data described below) had no effect on the level of core MerA expression, suggesting that any stabilizing interactions between the core and the NmerA domain in the full-length protein may simply be too weak to be effective when the proteins are detached.

As a further control before analysis of Hg^{2+} resistance, the glutathione deficiency of the *gshA*$^-$ mutant WB821 and the effect of protein expression on total cellular thiol content [RSH] were evaluated in a procedure using DTNB (*40*).

[5] The equilibrium in eq 4 can be formulated as $K_{eq3} = K_{formHgNmerA}/K_{formHg(SG)_2}$. Combining the lower estimate of 1.75×10^{-1} M for K_{eq3} with a lower estimate of $K_{formHg(SG)_2}$ of 10^{35} M^{-2} (3) yields a lower estimate for $K_{formHgNmerA}$ of 1.75×10^{34} M^{-1} or a $K_{dHgNmerA}$ of 6×10^{-35} M. Although a crude estimate, this is more realistic for a chelated Hg(dithiol) complex than the K_d value of 2 μM reported by Rossy et al. (*1*), obtained from titrations of their domain with $HgCl_2$. However, it should be noted that the lack of further spectral changes in their titrations after addition of 1 equiv of Hg^{2+}/protein even at their lowest protein concentration examined (3.5 μM) is indicative of a much lower, but indeterminable K_d value than the reported 2 μM. Furthermore, their value is actually an apparent K_d relative to $Hg(NR_3)_2^{2+}$ since it was measured under conditions with ca. 10 mM free Tris base in solution and amines are much stronger ligands than chloride [$K_{formHgCl_2} = 10^{13.2}$ M^{-2}; $K_{formHg(NR_3)_2} = 10^{17.5}$ M^{-2} (*4*)]. Combining their apparent K_d of 2 μM measured at 10 mM NR_3 with $K_{formHg(NR_3)_2} = 10^{17.5}$ M^{-2} indicates that $K_{dHgNmerA}$ measured in their experiments is much lower than 10^{-19} M, consistent with the lower estimated value here.

Table 5: MerA Expression and Cellular Thiol Content in WT and *gshA*$^-$ *E. coli* Cells

E. coli strain	MerA protein(s) (plasmid)	protein expression[a] (μM)		total cellular thiols (mM)	
		uninduced	induced	uninduced	induced
AB1157 (wild type)	none (none)	NA	NA	8.0 ± 0.3	NA
	full length[b] (pFull)	427 ± 142	1926 ± 1071	11.9 ± 1.6	11.4 ± 2.2
	catalytic core (pCore)	33 ± 17	150 ± 127	7.9 ± 2.0	8.0 ± 0.9
	core[c] with NmerA (pCN)	13	73	9.9 ± 1.4	9.2 ± 2.5
WB821 *gshA*$^-$	none (none)	NA	NA	4.0 ± 0.3	NA
	full length[b] (pFull)	390 ± 61	2047 ± 1347	6.1 ± 0.2	6.4 ± 0.7
	catalytic core (pCore)	24 ± 4	99 ± 1	3.8 ± 0.3	4.5 ± 0.4
	core[c] with NmerA (pCN)	16	120	4.8 ± 1.6	4.9 ± 1.0

[a] Full-length, proteolytically processed full-length, and catalytic core MerA were quantified by densitometric analysis of immunoblots. [b] For protein densitometry, full-length and processed MerA were combined. The unprocessed form was typically 50−90% of anti-MerA reactive material. [c] Value is for core only as detection of NmerA from cells in the gels was not possible due to the faint, diffuse band for this small protein and the limited amount of cell lysate that could be loaded on the gel.

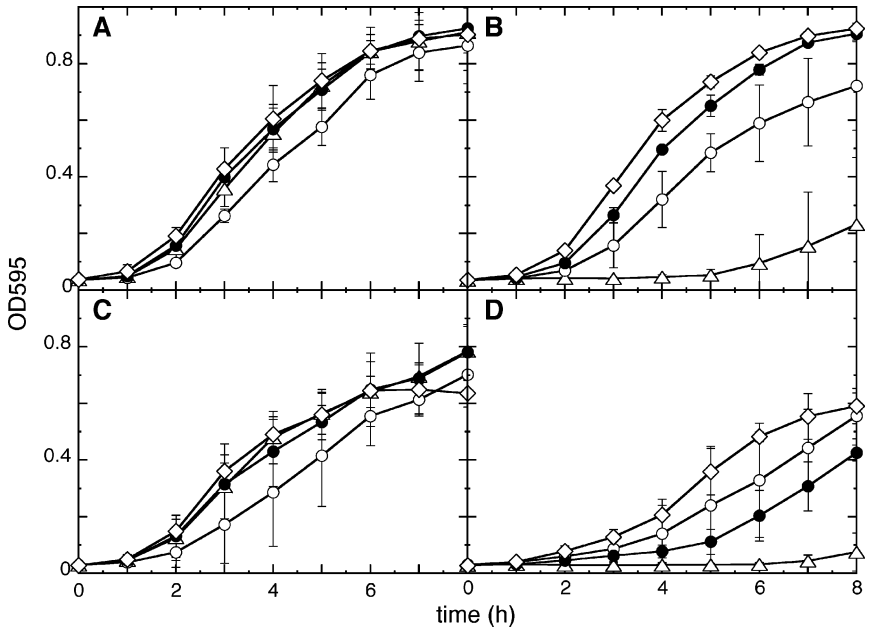

FIGURE 7: Liquid growth curves for *E. coli* strain AB1157 (wild type) (panels A and B) and its *gshA*$^-$ mutant strain WB821 (panels C and D) expressing various MerA proteins in the absence (A and C) or presence (B and D) of 15 μM $HgCl_2$. Key: (△) no MerA, (●) catalytic core MerA (pCore), (○) full-length MerA (pFull), and (◇) catalytic core MerA coexpressed with NmerA (pCN).

Intracellular glutathione concentration has been reported to average from 1 to 10 mM in *E. coli* (*53*, *54*). As summarized in Table 5, WB821 has 4−6 mM lower soluble [RSH] than the *gsh*$^+$ parent AB1157, consistent with the loss of GSH but retention of other soluble thiols such as cysteine and thioredoxin. The presence of pFull or pCN provokes a slight rise in [RSH] compared to pCore (reason not presently known), but protein induction causes no change in [RSH]. Thus, WB821 is deficient in glutathione, and expression of MerA proteins does not alter cellular [RSH] in any of the strains used.

To determine whether NmerA confers a phenotypic advantage against Hg(II) to cells deficient in glutathione, two methods were employed. The first, efficiency of plating (EOP), requires a single cell to be able to form a colony on selective media and is the most stringent test of a resistance phenotype. By EOP, we did not detect any mercury resistance conveyed by the full-length or core MerA proteins compared to the complete *mer* operon (Table S2). However, we could detect mercury resistance conferred by these proteins using liquid cultures, a less strenuous test based on differential growth of dilute cultures.

As summarized in Figure 7, $HgCl_2$ at 15 μM is toxic to both the *gshA*$^-$ mutant and its parent strain (triangles, Figure 7B,D), but cells with uninduced[6] levels of expressed proteins from pFull, pCore, or pCN tolerated this toxicity to varying degrees in both strains. In the absence of $HgCl_2$, the presence of the full-length construct pFull hindered the growth of both *gsh*$^+$ and *gshA*$^-$ strains, while pCore and pCN had no effect (Figure 7A,C), suggesting that the much higher level of full-length protein expression noted above (Table 5) may itself be a stress on the cells. Surprisingly, this effect appears to be augmented in glutathione-replete cells, where those carrying pFull and a higher load of full-length protein show some resistance but are more hindered than those expressing lower levels of core MerA from either pCore or pCN. Most important for the *gsh*$^+$ cells though is the observation that expression of core MerA alone provides sufficient protection to allow growth at nearly normal rates (Figure 7A,B), consistent with the in vitro results showing that the steady-

[6] For the phenotypic analysis, the cells were not induced for protein expression because high expression itself leads to erratic growth curves for cells expressing MerA.

state rate of turnover is nearly the same for full-length and core proteins when [GSH] is high (Table 2). In contrast, in the glutathione-deficient *gshA*$^-$ strain, the presence of NmerA in any form provides greater mercury resistance than that obtained from core MerA alone (Figure 7D). In this case, cells carrying pFull do provide greater protection than those carrying pCore, but those carrying pCN exhibit the greatest resistance, confirming that NmerA is coexpressed and is beneficial to cells deficient in GSH.

Conclusions. The combined results presented in this paper provide compelling evidence for a functional role of the highly conserved metal binding NmerA domain of mercuric ion reductases in the acquisition and delivery of Hg^{2+} to the catalytic core for reduction. Both the in vitro and in vivo results suggest that the presence of NmerA is of little importance as long as cells are replete with small molecular weight thiols such as GSH, consistent with the previous in vivo studies of the N-terminal di-Ala mutant of MerA in the full operon (*29*, *32*). However, if the thiol concentration drops, as occurs in the presence of various oxidative or other electrophilic stressors including Hg^{2+} (*55*), the presence of NmerA provides a substantial benefit for cell survival in the presence of Hg^{2+}. Thus, for organisms such as *P. aeruginosa* and *E. coli* that normally possess high concentrations of intracellular thiols, the NmerA domain may be thought of as an insurance policy, but one that apparently is used frequently enough for it to have been genetically maintained in a wide variety of organisms. Although it remains to be tested, NmerA may be particularly important under thiol-depleted conditions for rapid acquisition of Hg(II) from the transport protein MerT as suggested by a recent demonstration that the MerAa (NmerA) domain from *R. metallidurans* CH34 MerA can remove Hg(II) from a cytoplasmic peptide fragment of MerT (*56*). However, the results may also explain why MerA proteins from Gram-positive organisms with typically lower intracellular thiol concentrations (*54*), such as *Bacillus* sp., have two repeats of the NmerA domain (*17*, *57*). With the constant lower level of thiol in those cells, the presence of the appended high-affinity chelate of NmerA is likely to be more essential for rapid localization and transfer of Hg^{2+} to the core for reduction in order to prevent the toxic effects resulting from distribution to and inhibition of other proteins in the cell.

ACKNOWLEDGMENT

Mass spectral data were provided by the UCSF Mass Spectrometry Facility (A. L. Burlingame, Director) supported by the Biomedical Research Technology Program of the National Center for Research Resources, NIH NCRR RR01614. We thank the staff at BioCARS sector 14 beamlines at the Advanced Photon Source, Argonne National Laboratories, for their generous time commitments and support. Use of the Advanced Photon Source was supported by the Basic Energy Sciences, Office of Science, U.S. Department of Energy, under Contract W-31-109-Eng-38. Use of the BioCARS sector 14 was supported by the National Center for Research Resources, National Institutes of Health, under Grant RR07707. We also thank Yan Liu for assistance with the PDB deposition and two anonymous reviewers for their helpful comments on the manuscript.

SUPPORTING INFORMATION AVAILABLE

(1) Table S1, statistics of data collection and refinement for the X-ray crystal structures, (2) Figure S1, the electron density for the C-terminal region of the Tn*501* catalytic core and an overlay of *Bacillus* and Tn*501* C-termini, (3) Figure S2, data showing inhibition of the core reaction with Hg−NmerA by reduced NmerA, along with a description and Scheme S1 showing two possible mechanisms for inhibition, and (4) Table S2, efficiency of plating data. This material is available free of charge via the Internet at http://pubs.acs.org.

REFERENCES

1. Rossy, E., Champier, L., Bersch, B., Brutscher, B., Blackledge, M., and Coves, J. (2004) Biophysical characterization of the MerP-like amino-terminal extension of the mercuric reductase from *Ralstonia metallidurans* CH34, *J. Biol. Inorg. Chem. 9*, 49−58.
2. Miller, S. M. (1999) Construction of separate expression vectors for the catalytic core and the N-terminal metal binding domain of Tn501 mercuric ion reductase, in *Flavins and Flavoproteins 1999* (Ghisla, S., Kroneck, P., Macheroux, P., and Sund, H., Eds.) pp 863−870, Agency for Scientific Publications, Berlin.
3. Stricks, W., and Kolthoff, I. M. (1953) Reactions between mercuric mercury and cysteine and glutathione. Apparent dissociation constants, heats and entropies of formation of various forms of mercuric mercapto-cysteine and -glutathione, *J. Am. Chem. Soc. 75*, 5673−5681.
4. Dean, J. A. (1992) *Lange's Handbook of Chemistry*, 14th ed., McGraw-Hill, New York.
5. Foster, T. J. (1983) Plasmid-determined resistance to antimicrobial drugs and toxic metal ions in bacteria, *Microbiol. Rev. 47*, 361−409.
6. Vallee, B. L., and Ulmer, D. D. (1972) Biochemical effects of mercury, cadmium, and lead, *Annu. Rev. Biochem. 41*, 91−128.
7. Rensing, C., Ghosh, M., and Rosen, B. P. (1999) Families of soft-metal-ion-transporting ATPases, *J. Bacteriol. 181*, 5891−5897.
8. Miller, S. (1999) Bacterial detoxification of Hg(II) and organomercurials, in *Essays in Biochemistry* (Ballou, D. P., Ed.) pp 17−30, Princeton University Press, Princeton, NJ.
9. Silver, S. (1996) Bacterial resistances to toxic metal ions—a review, *Gene 179*, 9−19.
10. Silver, S., and Phung, L. T. (1996) Bacterial heavy metal resistance: new surprises, *Annu. Rev. Microbiol. 50*, 753−789.
11. Mukhopadhyay, R., and Rosen, B. P. (2002) Arsenate reductases in prokaryotes and eukaryotes, *Environ. Health Perspect. 110* (Suppl. 5), 745−748.
12. O'Halloran, T. V., and Culotta, V. C. (2000) Metallochaperones, an intracellular shuttle service for metal ions, *J. Biol. Chem. 275*, 25057−25060.
13. Cheesman, B. V., Arnold, A. P., and Rabenstein, D. L. (1988) Nuclear magnetic resonance studies of the solution chemistry of metal complexes. 25. Hg(thiol)3 complexes and Hg(II)-thiol ligand exchange kinetics, *J. Am. Chem. Soc. 110*, 6359−6364.
14. Schottel, J. L. (1978) The mercuric and organomercurial detoxifying enzymes from a plasmid-bearing strain of *Escherichia coli*, *J. Biol. Chem. 253*, 4341−4349.
15. Brown, N. L. (1985) Bacterial resistance to mercury—reductio ad absurdum? *Trends Biochem. Sci. 10*, 400−403.
16. Summers, A. O. (1986) Organization, expression, and evolution of genes for mercury resistance, *Annu. Rev. Microbiol. 40*, 607−634.
17. Barkay, T., Miller, S. M., and Summers, A. O. (2003) Bacterial mercury resistance from atoms to ecosystems, *FEMS Microbiol. Rev. 27*, 355−384.
18. Fox, B., and Walsh, C. T. (1982) Mercuric reductase. Purification and characterization of a transposon-encoded flavoprotein containing an oxidation−reduction-active disulfide, *J. Biol. Chem. 257*, 2498−2503.
19. Brown, N. L., Ford, S. J., Pridmore, R. D., and Fritzinger, D. C. (1983) Nucleotide sequence of a gene from the Pseudomonas transposon Tn501 encoding mercuric reductase, *Biochemistry 22*, 4089−4095.
20. Williams, C. H., Jr. (1992) Lipoamide dehydrogenase, glutathione redcutase, thioredoxin reductase, and mercuric ion reductase—a family of flavoenzyme transhydrogenases, in *Chemistry and*

Biochemistry of Flavoenzymes (Muller, F., Ed.) pp 123−211, CRC Press, Boca Raton, FL.
21. Williams, C. H., Arscott, L. D., Muller, S., Lennon, B. W., Ludwig, M. L., Wang, P. F., Veine, D. M., Becker, K., and Schirmer, R. H. (2000) Thioredoxin reductase two modes of catalysis have evolved, *Eur. J. Biochem. 267*, 6110−6117.
22. Schiering, N., Kabsch, W., Moore, M. J., Distefano, M. D., Walsh, C. T., and Pai, E. F. (1991) Structure of the detoxification catalyst mercuric ion reductase from *Bacillus* sp. strain RC607, *Nature 352*, 168−172.
23. Arnesano, F., Banci, L., Bertini, I., Ciofi-Baffoni, S., Molteni, E., Huffman, D. L., and O'Halloran, T. V. (2002) Metallochaperones and metal-transporting ATPases: a comparative analysis of sequences and structures, *Genome Res. 12*, 255−271.
24. Distefano, M. D., Moore, M. J., and Walsh, C. T. (1990) Active site of mercuric reductase resides at the subunit interface and requires Cys135 and Cys140 from one subunit and Cys558 and Cys559 from the adjacent subunit: evidence from in vivo and in vitro heterodimer formation, *Biochemistry 29*, 2703−2713.
25. Engst, S., and Miller, S. M. (1999) Rapid reduction of Hg(II) by mercuric ion reductase does not require the conserved C-terminal cysteine pair using $HgBr_2$ as the substrate, *Biochemistry 38*, 853−854.
26. Engst, S., and Miller, S. M. (1998) Rapid reduction of Hg(II) by mercuric ion reductase does not require the conserved C-terminal cysteine pair using $HgBr_2$ as the substrate, *Biochemistry 37*, 11496−11507.
27. Miller, S. M., Moore, M. J., Massey, V., Williams, C. H., Jr., Distefano, M. D., Ballou, D. P., and Walsh, C. T. (1989) Evidence for the participation of Cys558 and Cys559 at the active site of mercuric reductase, *Biochemistry 28*, 1194−1205.
28. Moore, M. J., Miller, S. M., and Walsh, C. T. (1992) C-Terminal cysteines of Tn501 mercuric ion reductase, *Biochemistry 31*, 1677−1685.
29. Moore, M. J., and Walsh, C. T. (1989) Mutagenesis of the N- and C-terminal cysteine pairs of Tn501 mercuric ion reductase: consequences for bacterial detoxification of mercurials, *Biochemistry 28*, 1183−1194.
30. Engst, S., and Miller, S. M. (1999) Alternative routes for entry of HgX_2 into the active site of mercuric ion reductase depend on the nature of the X ligands, *Biochemistry 38*, 3519−3529.
31. Fox, B. S., and Walsh, C. T. (1983) Mercuric reductase: homology to glutathione reductase and lipoamide dehydrogenase. Iodoacetamide alkylation and sequence of the active site peptide, *Biochemistry 22*, 4082−4088.
32. Brown, N. L., Shih, Y. C., Leang, C., Glendinning, K. J., Hobman, J. L., and Wilson, J. R. (2002) Mercury transport and resistance, *Biochem. Soc. Trans. 30*, 715−718.
33. Karplus, P. A., and Schulz, G. E. (1987) Refined structure of glutathione reductase at 1.54 Å resolution, *J. Mol. Biol. 195*, 701−729.
34. Distefano, M. D., Au, K. G., and Walsh, C. T. (1989) Mutagenesis of the redox-active disulfide in mercuric ion reductase: catalysis by mutant enzymes restricted to flavin redox chemistry, *Biochemistry 28*, 1168−1183.
35. Otwinowski, Z., and Minor, W. (1997) Processing of X-ray diffraction data collected in oscillation mode, *Methods Enzymol. 276A*, 307−326.
36. Brünger, A. T., Adams, P. D., Clore, G. M., DeLano, W. L., Gros, P., Grosse-Kunstleve, R. W., Jiang, J.-S., Kuszewski, J., Nilges, N., Pannu, N. S., Read, R. J., Rice, L. M., Simonson, T., and Warren, G. L. (1998) Crystallography and NMR system (CNS): A new software system for macromolecular structure determination, *Acta Crystallogr. D54*, 905−921.
37. Jones, T. A., Zou, J.-Y., Cowan, S. W., and Kjeldgaard, M. (1991) Improved methods for the building of protein models in electron density maps and the location of errors in these models, *Acta Crystallogr. A47*, 110−119.
38. Riddles, P. W., Blakeley, R. L., and Zerner, B. (1979) Ellman's reagent: 5,5′-dithiobis(2-nitrobenzoic acid)—a reexamination, *Anal. Biochem. 94*, 75−81.
39. Holmgren, A., and Reichard, P. (1967) Thioredoxin 2: cleavage with cyanogen bromide, *Eur. J. Biochem. 2*, 187−196.
40. Owens, C. W., and Belcher, R. V. (1965) A Colorimetric micro-method for the determination of glutathione, *Biochem. J. 94*, 705−711.
41. Ausubel, F. M. (1987) *Current protocols in molecular biology*, Greene Publishing Associates, J. Wiley, Brooklyn, NY, and Media, PA.
42. Neidhardt, F. C., and Curtiss, R. (1996) Chemical composition of *Escherichia coli*, in *Escherichia coli* and *Salmonella*: cellular and molecular biology (Neidhart, F. C., et al., Eds.) 2nd ed., pp 13−16, ASM Press, Washington, DC.
43. Sandstrom, A., and Lindskog, S. (1987) Activation of mercuric reductase by the substrate NADPH, *Eur. J. Biochem. 164*, 243−249.
44. Schiering, N. (1991) Doctoral Thesis, University of Heidelberg, Heidelberg, Germany.
45. Gill, S. C., and von Hippel, P. H. (1989) Calculation of protein extinction coefficients from amino acid sequence data, *Anal. Biochem. 182*, 319−326.
46. Serber, Z., Keatinge-Clay, A. T., Ledwidge, R., Kelly, A. E., Miller, S. M., and Dotsch, V. (2001) High-resolution macromolecular NMR spectroscopy inside living cells, *J. Am. Chem. Soc. 123*, 2446−2447.
47. Sahlman, L., and Jonsson, B. H. (1992) Purification and properties of the mercuric-ion-binding protein MerP, *Eur. J. Biochem. 205*, 375−381.
48. Distefano, M. D. (1989) Ph.D. Thesis, Massachusetts Institute of Technology, Cambridge, MA.
49. Marshall, J. L., Booth, J. E., and Williams, J. W. (1984) Characterization of the covalent mercury (II)-NADPH complex, *J. Biol. Chem. 259*, 3033−3036.
50. Eklund, H., Gleason, F. K., and Holmgren, A. (1991) Structural and functional relations among thioredoxins of different species, *Proteins 11*, 13−28.
51. Danon, A. (2002) Redox reactions of regulatory proteins: do kinetics promote specificity?, *Trends Biochem. Sci. 27*, 197−203.
52. Latinwo, L. M., Donald, C., Ikediobi, C., and Silver, S. (1998) Effects of intracellular glutathione on sensitivity of *Escherichia coli* to mercury and arsenite, *Biochem. Biophys. Res. Commun. 242*, 67−70.
53. Ding, H., and Demple, B. (1996) Glutathione-mediated destabilization in vitro of [2Fe-2S] centers in the SoxR regulatory protein, *Proc. Natl. Acad. Sci. U.S.A. 93*, 9449−9453.
54. Fahey, R. C., Brown, W. C., Adams, W. B., and Worsham, M. B. (1978) Occurrence of glutathione in bacteria, *J. Bacteriol. 133*, 1126−1129.
55. Lund, B. O., Miller, D. M., and Woods, J. S. (1993) Studies on Hg(II)-induced H_2O_2 formation and oxidative stress in vivo and in vitro in rat kidney mitochondria, *Biochem. Pharmacol. 45*, 2017−2024.
56. Rossy, E., Seneque, O., Lascoux, D., Lemaire, D., Crouzy, S., Delangle, P., and Coves, J. (2004) Is the cytoplasmic loop of MerT, the mercuric ion transport protein, involved in mercury transfer to the mercuric reductase?, *FEBS Lett. 575*, 86−90.
57. Wang, Y., Moore, M., Levinson, H. S., Silver, S., Walsh, C., and Mahler, I. (1989) Nucleotide sequence of a chromosomal mercury resistance determinant from a *Bacillus* sp. with broad-spectrum mercury resistance, *J. Bacteriol. 171*, 83−92.
58. Apontoweil, P., and Berends, W. (1975) Isolation and initial characterization of glutathione-deficient mutants of *Escherichia coli* K 12, *Biochim. Biophys. Acta 399*, 10−22.
59. Foster, T. J., Nakahara, H., Weiss, A. A., and Silver S. (1979) Transposon A-generated mutations in the mercuric resistance genes of plasmid R100-1, *J. Bacteriol. 140*, 167−181.
60. Gambill, B. D., and Summers, A. O. (1985) Versatile mercury-resistant cloning and expression vectors, *Gene 39*, 293−297.

BI050519D